AL/PDO Forces a Decadal Subsurface Spiciness Propagating Mode in the North Pacific

Sieu-Cuong San[1] and Yu-heng Tseng[1,2]

[1]Institute of Oceanography, National Taiwan University, Taipei, Taiwan.
[2]Ocean Center, National Taiwan University, Taipei, Taiwan.
Corresponding author: Y. Tseng (tsengyh@ntu.edu.tw)

Key Points:

- AL/PDO forces a decadal subsurface spiciness propagating mode characterized by a dipole pattern via changes in net surface heat flux.
- Subduction and reemergence are responsible for eastern midlatitude isopycnal spiciness variability.
- Spice injection and anomalous advection across mean spiciness gradient are responsible for subtropical interior spiciness generation.

Abstract

Analysis of observational data reveals the existence of a decadal spiciness mode that involves ocean-atmosphere coupling in the North Pacific. Specifically, the Aleutian Low (AL) which is the dominant atmospheric forcing of the Pacific Decadal Oscillation (PDO) drives a dipole pattern of positive and negative spiciness anomalies in the eastern midlatitude and subtropics, respectively. These anomalies then propagate equatorward along a deflected route defined by the mean acceleration potential. The positive anomaly can be observed at 14^0N after 7 years of propagation while the downstream negative anomaly can be tracked to 10^0N after 3 years of its appearance. In addition, a negative spiciness anomaly appears in the midlatitude, followed by the formation of the positive 2 years later. It takes a similar pathway toward the tropics. Further analysis suggests the potential impact of extratropical signals on tropical climate variability while the tropical surface signatures also feedback to the extratropical spiciness variability. These, in turn, potentially lead to a decadal climate oscillation in the North Pacific involving both atmospheric and oceanic bridges.

The dominant physical processes responsible for the subsurface spiciness variability are significantly different between the eastern midlatitude and subtropical North Pacific. In the midlatitude, isopycnal spiciness variability exhibits similar characteristics as the temperature variation at around 60-120m depth which is mainly produced via the subduction and reemergence mechanisms. In contrast, subtropical interior spiciness variability follows the evolution of salinity anomalies at around 120-240m. Both injection and anomalous advection across mean spiciness gradient likely dominate the subtropical isopycnal spiciness variability.

Plain Language Summary

The PDO and its dominant atmospheric forcing, the AL, have profound influences on global climate variability on a wide range of temporal scales. However, the connection between AL/PDO and subsurface spiciness evolution in the North Pacific has not been thoroughly investigated. Therefore, using statistical analysis, we find that AL/PDO forces a dipole pattern of spiciness anomalies in the midlatitude and subtropics by changing the net surface heat flux anomalies. These patterns can affect the tropical climate variability through the subsurface ocean pathways at interannual to decadal time scales. Further analysis suggests the potential two-way interaction between extratropical subsurface signal and tropical climate variability which can lead to a decadal climate oscillation in the North Pacific.

1 Introduction

The low-frequency dynamics of subsurface temperature/salinity anomalies in the eastern Pacific Oceans have long been an active theme of research due to their important role in connecting the extratropics with the tropics (Gu & Philander, 1997; Schneider, 2000, 2004). After a positive temperature anomaly is formed in the subtropical North Pacific, it is then advected adiabatically by the mean current westward and equatorward along isopycnal surfaces toward the tropical region (Kolodziejczyk & Gaillard, 2012; Sasaki et al., 2010). Along the equator, the anomaly flows east by the Equatorial Undercurrent (EUC), upwells, and warms the surface in the central-eastern equatorial Pacific. The surface warming also concurrently relaxes the local easterlies. Therefore, this warming is further enhanced via the positive Bjerknes feedback. Subsequently, the equatorial warming forces deep atmospheric convection that propagates into the extratropical North Pacific through the Pacific-North American (PNA) teleconnection (Alexander, 1990, 1992). This atmospheric perturbation modulates the strength of the AL, zonal wind anomalies, and hence turbulent heat flux in the midlatitude. Eventually, a negative subsurface temperature anomaly is generated and then propagates along a similar path of the positive anomaly toward the equator. This forms a decadal climate variability in the North Pacific with the time scale determined by the equatorward ventilation of the anomalous signals (Gu & Philander, 1997).

The generation of subsurface temperature/salinity anomalies can be classified into two distinct mechanisms: subduction and injection. The subduction occurs when an isopycnal exposes to the surface and allows sea surface signals to follow the outcrop line toward the interior ocean (Kolodziejczyk & Gaillard, 2012; Nonaka & Sasaki, 2007). Therefore, the meridional displacement of the outcrop line which is governed by the compensated contribution of SST and SSS determines the positive or negative signature of the anomaly on the isopycnal surface (Nonaka & Sasaki, 2007). This mechanism generates anomaly locally, i.e., just below the position of the outcrop line. The injection mechanism (spice injection), on the other hand, generates subsurface anomaly further equatorward away from the isopycnal outcrop position and is responsible for positive anomaly (Kolodziejczyk & Gaillard, 2012; Luo et al., 2005; Wang & Luo, 2020; Yeager & Large, 2004). The injection occurs when the examined isopycnal does not expose to the surface, but the large unstable vertical salinity gradient in conjunction with weak stratification in winter favors convective mixing at the base of the mixed layer (Yeager & Large, 2004). As a result, the saline water is injected to subsurface and creates a highly compensated layer of temperature and salinity, termed spiciness anomaly, at the base of the mixed layer (Wang & Luo, 2020; Yeager & Large, 2004). Furthermore, subsurface anomaly generation involving atmospheric stochastic forcing is also proposed. In particular, the ocean filters the overlying atmospheric noise (Hasselmann, 1976) resulting in a large-scale first baroclinic mode pressure response. The anomalous geostrophic advection then crosses the mean spiciness gradient which in turn generates low-frequency subsurface spiciness variability (Kilpatrick et al., 2011). Isopycnal spiciness anomaly formation via this mechanism has also shown to dominate in model simulation, leading to a decadal spiciness mode in the tropical North Pacific (Schneider, 2000).

The spiciness variable, which is often represented as temperature or salinity on a certain isopycnal surface (Kolodziejczyk & Gaillard, 2012; Li et al., 2012; Zeller et al., 2021), has been increasingly employed in recent literature to investigate low-frequency climate variability. Initially, spiciness (or potential spicity) is constructed as a state variable to characterize the rest

information of thermodynamics not included by the potential density. Therefore, isolines of spiciness are required to be orthogonal with potential density in the T-S diagram (Huang, 2011; Huang et al., 2018; Munk, 1981; Stommel, 1962; Veronis, 1972). Spiciness defined this way is assumed to be dynamically passive, accurately measuring mixing along isopycnal surfaces (Veronis, 1972). However, later studies identified that such orthogonal constraint is ambiguous because the scaling in the axes of the T-S diagram can vary in tandem with the thermal expansion and haline contraction coefficients (Flament, 2002; Jackett & Mcdougall, 1985; McDougall & Krzysik, 2015). In addition, the passive behavior of spiciness lies in its variations along isopycnal surfaces but not the inherited property of any thermodynamic variable (McDougall et al., 2021; McDougall & Krzysik, 2015). McDougall and Krzysik (2015) sacrificed the orthogonal enforcement but strictly required the variation of spiciness along isopycnal surfaces be proportional to the isopycnal water-mass variations, expressed in density unit. A solid theory available for the construction of spiciness so far is still a matter of ongoing debate and largely evolving along two main streams: orthogonality (Huang et al., 2021) and nonorthogonality (McDougall et al., 2021) with the potential density in the T-S diagram.

The corridor for the eastern extratropical subsurface signals propagating toward the equator is via the so-called subtropical-tropical cell (STC) (Liu, 1994; McCreary & Lu, 1994), a shallow overturning circulation confined to the upper 500 m, consisting of the subsurface equatorward branch, equatorial upwelling branch and poleward flow in the surface Ekman layer (Capotondi et al., 2005; Schott et al., 2004). Past observational and modeling studies have demonstrated the existence of the STC and drawn an overall picture of the characteristics of the communication windows between the equatorial thermocline and midlatitude subduction regions (Fine et al., 1987; Liu & Huang, 1998; Liu et al., 1994; Lu & McCreary, 1995; Lu et al., 1998; McPhaden & Fine, 1988; Rothstein et al., 1998). Depending upon the longitude at which subduction occurs, the anomaly advected within the lower branch of the STC can reach the equator via two distinct pathways. In the central North Pacific, the subducted water first flows southwestward to arrive at the western boundary and then turns southward toward the equator by the low latitude western boundary undercurrent (the western boundary pathway, WBP). In contrast, water subducted in the eastern subtropical basin first flows southwestward and then directly feeds into the EUC in the central-eastern equatorial Pacific (the interior pathway, IP). Though many dynamical aspects of the two pathways have been well documented in previous literature, a comprehensive separation of the WBP and IP remains challenging. Up to now, most of the studies mainly employ virtual or Montgomery streamfunction evaluated on isopycnal surfaces to differentiate the WBP and IP (Fukumori et al., 2004; Johnson & McPhaden, 1999; Li et al., 2012). In addition, the preferential pathway that the subducted anomaly takes to reach the equator as well as the relative contribution of Northern versus Southern Hemisphere WBP and IP remain unclear. In the North Pacific, there is a barrier associated with the high potential vorticity induced by positive Ekman pumping in the northeastern Pacific, which inhibits the direct communication of lower layer water from the subtropics to the tropics. Therefore, the anomaly has to flow through a more convoluted route to reach the equator (Johnson & McPhaden, 1999; Lu et al., 1998; Rothstein et al., 1998) or almost flow toward the western boundary to join the EUC (Fukumori et al., 2004; Furue et al., 2015; Lu & McCreary, 1995). Furthermore, a considerable amount of North Pacific ventilated thermocline water heads into the Indian Ocean via the Indonesia Throughflow which strongly reduces the exchange flux of subtropical water to the western equatorial region (Lee et al., 2002; Nie et al., 2016; Rodgers et al., 1999). In the South Pacific, however, due to the absence of such a high potential vorticity barrier, the anomaly

can take a direct pathway toward the equator in the interior ocean. As a result, the South Pacific contributes significantly more subtropical water to the tropics than the North Pacific does via IP (Fukumori et al., 2004; Goodman et al., 2005; Johnson & McPhaden, 1999). Also, as the distance coverage of the anomaly in the South Pacific along the IP is much shorter than its Northern counterpart, the impact of the South Pacific subtropical anomaly on the tropical climate variability appears to be of greater magnitude and shorter lead time (Kolodziejczyk & Gaillard, 2012; Kuntz & Schrag, 2018; Luo et al., 2005; O'Kane et al., 2014; Tatebe et al., 2013; Yang et al., 2005).

One appealing question is whether the advection of spiciness anomaly by mean current along IPs and WBPs can effectively migrate to the equator and impact the tropical climate variability. Modeling (Fukumori et al., 2004; Giese et al., 2002; Pierce et al., 2000; Schneider, 2000; Schneider et al., 1999b; Yeager & Large, 2004) as well as observational studies (Schneider et al., 1999a; Zhang & Liu, 1999) have obtained ambiguous conclusions regarding such propagating signal from the extratropical subduction zone in both hemispheres. On the one hand, some studies demonstrated that the magnitude of spiciness anomaly diminishes significantly during the propagation (Kolodziejczyk & Gaillard, 2012; Liu & Shin, 1999; Sasaki et al., 2010) and likely cannot arrive the western equatorial Pacific (Hazeleger et al., 2001; Schneider et al., 1999a). On the other hand, some studies found that the spiciness anomaly can spread to the equator via the IP (Li et al., 2012; Luo et al., 2005) and/or WBP (Kolodziejczyk & Gaillard, 2012; Luo et al., 2005; Sasaki et al., 2010; Yeager & Large, 2004) but at much reduced amplitude. Moreover, the relative contribution of the mean advection of spiciness anomaly along IP versus WBP at each hemisphere to the low-frequency signal peak in the equator is subject to event dependence. Employing an ocean general circulation model (OGCM) combined with a Lagrangian particle simulator forced with climatological surface conditions, Zeller et al. (2021) showed one positive event peak in the subsurface equator is mainly contributed by Southern Hemisphere water traveling along the IP while another negative event peak is primarily caused by water traveling via the WBP in the Northern Hemisphere. Although many efforts have been made in the role of extratropical signals on the interannual to decadal tropical variability, a thorough understanding regarding the fate of SSAs during the equatorward propagation and their impact on Pacific climate variability as well as the dominant physical processes responsible for the isopycnal spiciness variability is still unclear.

In this study, the dominant propagating pattern of low-frequency SSAs in the North Pacific is characterized and linked with the PDO by employing two different observational datasets. In addition, we further examine the processes responsible for isopycnal spiciness variability in the midlatitude and subtropics. This paper is organized as follows. Section 2 describes the data and the method utilized. Section 3 presents the main result of the study followed by discussion and concluding remarks in Section 4 and Section 5, respectively.

2 Data and Methodology

For the ocean subsurface temperature and salinity, we use the latest EN.4.2.2 in the ‘EN’ series of data sets from the Met Office Hadley Centre (Good et al., 2013), 1-degree horizontal grid over 42 non-uniform spaced depth levels spanning from 1900 to present at monthly intervals. Four ensemble members are available in EN.4.2.2. EN.4.2.2.g10 (hereinafter referred to as EN422) is chosen for our analysis while the results extracted from the other three ensembles are qualitatively consistent and similar. All available sources of oceanographic

measurements are adopted in this product, primarily from the WOD09. In addition, the gridded Grid Point Value of the Monthly Objective Analysis (MOAA GPV) (Hosoda et al., 2008) is also used to compare the evolution of subsurface anomalies during 2001-2019. The MOAA GPV is constructed mainly from Argo floats in combination with buoy measurements and casts of research cruises. The horizontal resolution is 1° on standard pressure levels between 10 and 2000 dbar. For the atmospheric field, the sea level pressure (SLP), SST, and 10-m wind data from the ERA5 (Hersbach et al., 2020) are used. To be consistent with atmospheric data, our analysis uses the period of 1979 to 2019 except for MOAA GPV which is analyzed from 2001 to 2019.

The temperature and salinity are first converted to conservative temperature (CT) and absolute salinity (SA) based on the TEOS-10 before calculating spiciness following the method proposed by Jackett and Mcdougall (1985) and McDougall and Krzysik (2015):

$$\int_{\rho^{\Theta}} d\tau = 2\int_{\rho^{\Theta}} \left.\frac{\partial \rho^{\Theta}}{\partial S_A}\right|_{\Theta,p_r} dS_A \qquad (1)$$

$$\tau_0\left(S_A,\Theta\right) = \tau_u \sum_{j=0}^{6}\sum_{k=0}^{6} A_{jk} s^j y^k \qquad (2)$$

where τ is spiciness, Θ is CT, ρ is potential density, p_r is reference pressure, τ_0 is spiciness referenced to 0 dbar, τ_u = 1 kg m^{-3}, A_{jk} are the coefficients of the polynomials for spiciness, s is the nondimensional salinity, and y is the nondimensional temperature (see McDougall and Krzysik (2015) for more details). The spiciness in pressure coordinate is then transformed to sigma coordinate by linear interpolation on the isopycnal range σ_θ = 25-26 with $\Delta\sigma_\theta$ = 0.01 kgm^{-3}. To remove the impacts of annual cycle, the interpolated data is filtered with a 13-month running mean. We also analyze the spiciness based on the definition of Huang et al. (2018). The results are qualitatively similar despite some small differences in the magnitude of the anomalies are present.

To account for the pathway connecting extratropics with the tropics, we calculate the mean acceleration potential (AP), referenced to 2000 dbar (McDougall & Klocker, 2010). It is then interpolated to sigma coordinate and low-pass filtered with a 13-month running mean. In this study, the IP and WBP are not explicitly separated. Here, we define the North Pacific Pathway (hereinafter referred to as NPP) as the passage between the AP contours of 19.7- and 21 m^{2}s^{-2} to describe the propagation features.

The temporal and spatial characteristics of low-frequency spiciness variability are investigated using a CEOF analysis (Barnett, 1983; Horel, 1984) performed in the North Pacific (0-60^{0}N, 120^{0}E-80^{0}W). The advantage of CEOF over traditional empirical orthogonal function (EOF) analysis lies in its ability to extract propagating properties in the data by providing not only the amplitude but also the potential phase change. Given the propagative nature of isopycnal spiciness anomalies, this method can reveal important propagation property relating to the fate of spiciness variability (see Text S1 for the detail).

3 Results

3.1 Characteristics of low-frequency spiciness variability

The CEOF analysis of spiciness anomalies between 25-26 σ_θ had identified the dominant mode of low-frequency variability in the North Pacific. This mode accounts for about 28% and

52% of the total spiciness variance in the EN422 and MOAA GPV datasets, respectively (Figures 1a and 1b). It is significantly distinguished from the rest modes and exhibits the most prominent propagating feature (Figures 1c, 1d and 2). Therefore, we focus entirely on the first CEOF mode (CEOF1) in this study. The spatial amplitude of CEOF1 is similar between the EN422 and MOAA GPV although the latter shows weaker magnitude in the eastern midlatitude (Figures 1a and 1b). In general, CEOF1 exhibits maximum variability equatorward from the outcropping area, centering at 38^0N, 140^0W. The associated magnitude reaches 0.12 kg m^{-3} in the center of action but decreases considerably downstream along the NPP. This area of maximum spiciness variability is consistent to that identified in Li et al. (2012) based on the potential temperature between 25-25.5 σ_θ. While CEOF1 of the present study possesses only one center of maximum variability in the extratropics, Li et al. (2012) showed the other secondary variability in the eastern subtropical region around 20^0N east of 130^0W. Compared to the CEOF1 of interannual salinity anomalies evaluated on the σ_θ=25.5 surface of Kolodziejczyk and Gaillard (2012), the spiciness signal in the present study is much more coherent and stronger, and the center of action expands further northward to about 50^0N (Figures 1a and 1b). These differences may ascribe to the isopycnal levels as well as the thermodynamic variable employed for the analysis. The two previous studies mainly evaluate the anomalies between σ_θ=25-25.5 which are shallower than the isopycnal levels considered here.

A propagating signal can be seen from the increasing spatial phase of CEOF1 along the NPP (Figures 1c and 1d). The abrupt zonal change of phase around 38^0N coincides with the large variance of the first mode. At lower latitudes, the phase structure is strongly modulated by the turn to the eastern edge of the pathway where the potential vorticity barrier (Lu & McCreary, 1995) hinders the direct equatorward transport from the extratropics to the tropics.

The propagating characteristics of the first and all CEOF modes are assessed by reconstructing the spiciness anomalies on the Hovmöller diagram along the NPP (Figure 2). During 1979-2019, there are episodes of positive and negative spiciness anomalies that occur in the extratropical North Pacific (Figure 2a). The alternative anomalies (two negative and one positive) during 2003-2011 have previously been reported (Kolodziejczyk & Gaillard, 2012; Li et al., 2012; Sasaki et al., 2010) (Figure 2). In addition, two major spiciness events of opposite signs that emerge from 2012 onwards: one negative anomaly appeared in 2012-2013 and the other positive anomaly originated in 2014-2015. Our results suggest that considering deeper isopycnal levels can characterize the isopycnal spiciness occurrence (variability) from the high latitude region at least one to two years in advance compared to the previous studies.

The reconstructed spiciness anomalies from CEOF1 show a clear pattern of equatorward propagation along the NPP with the strongest variability observed poleward of 24^0N, consistent with the spatial amplitude distribution (Figures 1a, 1b, and 2a). The magnitude is gradually reduced as expected. In addition, the equatorward propagation of prominent spiciness anomalies from 40^0N to 10^0N lasts for about 8 years (Figure 2a) which is consistent with the temporal phase change (Figure 3). This time scale is in good agreement with the estimated time scale of 7-8 years for the extratropical origin of subsurface signals to reach the tropics (Kolodziejczyk & Gaillard, 2012; Schneider et al., 1999a). Previous observational study also suggested that the subducted thermal anomalies originated in the central North Pacific propagating along the WBP can only be tracked no further than 18^0N in the western Pacific (Schneider et al., 1999a). In contrast, our study reveals the propagation signals along the NPP can reach further equatorward to 10^0N (Figure 2). The discrepancy may attribute to the effectiveness of spiciness over the

temperature (and salinity) variable in accounting for low-frequency variability (Wang & Luo, 2020) because thermal (salinity) anomalies are subject to be modulated both by conservative and nonconservative processes during the propagation (Tailleux et al., 2005).

There is a substantial difference between the spiciness signals before and after 1998/1999 (Figure 2), a period when the North Pacific SST and the relevant atmospheric condition changed abruptly (Lyon et al., 2014), which is often referred to climate regime shift occurring in the winter of 1998/1999. This shift has resulted in a shorter period in the persistence of the cold/warm phases associated with the PDO since 1998/1999 in which the duration of a particular warm/cold phase lasts for only several years compared to the prolonged warm condition before the 1998/1999 regime shift (Figure 3). For comparison, the time evolution of the first principal component (PC1) of spiciness anomalies is shown in Figure 3. While the imaginary component almost varies in tandem with the PDO index, there is a time lag between the real part with the PDO in which the peak of the latter leads the peak of the former for over one year. The in-phase relation can be further confirmed by the strong correlation when PDO leads PC1 (real) of spiciness anomalies around 18-24 months (Figure 4a), suggesting the relevance between the two leading modes of surface and subsurface oceanic variability in the North Pacific (Figure 3). This will be elaborated more in the next section.

3.2 Forcing mechanism

Motivated by the linkage between PDO and the PC1 (real) of spiciness anomalies, we further investigate the role of PDO in forcing subsurface variability in the extratropical North Pacific. Defined as the leading EOF of monthly SSTAs poleward of 20^0N (Mantua et al., 1997), the spatial pattern of the positive PDO phase is characterized by a positive anomaly extending from the high-latitude toward the equator along the west coast of North America combining a negative anomaly in the central Pacific (Figure 5a). As the SLP and 10m-wind vector anomalies are regressed onto the PDO index, an intense cyclonic circulation corresponding with the strengthening of the AL can be found in the North Pacific (Figure 5b). In addition, the interannual variability of the AL (defined as the principal component of leading EOF of interannual SLP anomalies (SLPAs) between 20^0-60^0N, 120^0E-80^0W) is strongly correlated with PDO, reaching a simultaneous correlation of 0.63 and as high as 0.68 when AL leads the PDO for 3 months (Figure 5c). This result is consistent with previous study (Schneider & Cornuelle, 2005).

Comparing the spatial structure of CEOF1 (Figures 1a and 1b) and the PDO pattern (Figure 5a) accompanied by its atmospheric forcing (Figure 5b), we find that the region of maximum spiciness variability coincides with the south-eastward extension of positive temperature anomaly below the center of AL. As the SSTAs are regressed onto the PC1 of spiciness anomalies (Figure S1), the resulting pattern is similar to the positive phase of the PDO. The role of the PDO forcing is further confirmed by the lead-lag correlation between the PDO index and the PC1 (real) of spiciness anomalies (Figure 4a). As expected, the highest correlation obtained when the PDO leads the spiciness anomalies for +22 months. This characteristic is not only present in the short-term but also in the long-term datasets with very high correlations, 0.92 and 0.72 for MOAA GPV and EN422, respectively. In addition, at negative lag months, the PC1s do not possess any significant correlations with the PDO index. These further demonstrate that PDO actively forces the spiciness anomalies while the latter responds passively.

To demonstrate the role of the PDO forcing, we regress the reconstructed spiciness anomalies from the CEOF1 with the PDO index at 22-month lag (highest correlation between the PDO and the associated PC1) on Figure 6a. The spatial pattern of CEOF1 associated with the real part is also presented on Figure 6b. The strongest positive variability in the eastern midlatitude is largely explained by the PDO forcing. In addition, there is another region of negative anomalies associated with the PDO forcing that centers on 20^0N, 145^0W. The defined NPP almost lies in the region of spiciness variability explained by the PDO forcing, thus can be employed to depict the propagation of spiciness anomalies from the source region toward the tropics.

Having established the strong relationship between the PDO and SSAs, it is therefore interesting to see how the spiciness signals evolve after the forcing of PDO. Figure 4b shows the lead-lag correlation between the reconstructed spiciness anomalies of CEOF1 averaged along the NPP and the PDO index. Consistent with the regression in Figure 6a, the derived lag correlation shows an equatorward evolving positive (negative) pattern that originates in the midlatitude (subtropics). The robustness of the PDO in forcing subsurface spiciness propagating mode can reach approximately 14^0N after 7 years (positive anomaly). The negative anomaly that formed in the eastern subtropics can propagate further equatorward, reaching 10^0N roughly after 3 years.

The equatorward subsurface propagation is a key process in modulating tropical climate variability at decadal time scales (Gu & Philander, 1997; Schneider, 2000). We further examine the PDO-forced propagating characteristic of subsurface by regressing the reconstructed spiciness anomalies of CEOF1 with the PDO index from no lag (lag 0) to 7 years later (Figure 7). A simultaneous dipole pattern of spiciness variability is formed associated with the PDO forcing at no lag: positive in the midlatitude centering at 40^0N, 135^0W and negative in subtropics centering at 22^0N, 130^0W. Afterward, the two anomalous signals propagate equatorward along the NPP. The positive spiciness anomaly not only propagates downstream but also strengthens until 4 years later (lag 48). It then weakens subsequently and continues to propagate until reaching 14^0N after 7 years (lag 84). The other negative anomaly formed in the subtropical eastern Pacific can also be observed 3 years later (lag 36) around 10^0N with a much stronger magnitude than the above positive anomaly arriving 14^0N. In addition, another negative anomaly (center at 40^0N, 150^0W) is formed alternatively in the midlatitude around 2 years later (lag 24). It then gradually amplifies (Stephens et al., 2001) and follows the similar pathway to the positive one to approach the western tropics (see also Figure 2a). This in turn creates a decadal cycle of equatorward ventilation, similar to the hypothesis of Gu and Philander (1997). Further analysis of the spectrum of the PC1 (real) confirms the robustness of this propagating mode as there is a significant peak (above the 99% red noise confidence level) at around 5-year, similar to the spectral peak of the PDO (Figure 8).

There is consistent migration of the subtropical negative signal to the interior central Pacific (lag 12 to lag 48, Figure 7). This off-equatorial signal propagation is consistent with the result of Li et al. (2012). The migration of the midlatitude signal toward the ocean interior, however, is not clearly observed compared to its downstream counterpart. The equatorward migration of the anomalies along the NPP at the western boundary is hard to detect clearly due to the coarse resolution and short period of the observational record employed although there is negative signal observed in the western boundary consistently propagates eastward at lag +12 to lag +60.

The above analysis has identified the role of PDO in forcing SSAs in both midlatitude and subtropical North Pacific. The AL, the dominant winter atmospheric circulation pattern in the North Pacific (Yu & Kim, 2011), has been demonstrated a primary driver of the PDO (Figure 5). We further investigate the connection between SSAs and the dominant atmospheric forcing of the PDO. Figure 9 shows the regression of SLP, 10m-wind vector, and net surface heat flux (positive downward) anomalies with the PC1 (real) of spiciness mode at lag +22 months. As expected, the midlatitude positive spiciness anomalies are associated with the strengthening of the AL through the change of PDO (Figures 6a and 9a). Previous studies suggested that the cyclonic wind anomalies associated with the intensified AL produce downward heat flux along the west coast of North America (Yu & Kim, 2011), consistent with the band of positive Qnet in the eastern midlatitude in Figure 9b. This pattern is coincident with the positive SSAs in Figure 6. Therefore, our results confirm the strengthening (weakening) of the AL drives a positive (negative) Qnet anomaly in the eastern midlatitude, forcing the corresponding positive (negative) SSAs.

3.3 Formation of isopycnal spiciness anomalies

The generation of SSAs in the eastern extratropical South Pacific can be quantified in terms of both subduction (Nonaka & Sasaki, 2007) and injection (Kolodziejczyk & Gaillard, 2012; Wang & Luo, 2020; Yeager & Large, 2004). However, the formation of isopycnal spiciness anomalies in the eastern subtropical North Pacific (25-33^{0}N, 150-135^{0}W) can only be ascribed in part to the injection during boreal winter (Katsura, 2018). In contrast, the subduction is proposed for isopycnal temperature variability in the central midlatitude North Pacific (Schneider et al., 1999a). As a result, whether the subduction or spice injection can explain the anomalies observed along the isopycnals of 25-26 kg m^{-3} is still unclear.

The PDO-forced subsurface variability results in spiciness anomalies of opposite sign in the midlatiude and subtropics. This suggests that different physical processes are involved in the formation of these spiciness anomalies. Therefore, we investigate the positive signal in the midlatitude (the red box, Figure 7) and the negative signal in the subtropics (the blue box, Figure 7) separately to identify the governing generation mechanisms in the two regions.

In general, subsurface spiciness evolution can be determined by the combined vertical variations of CT and SA. In addition, surface oceanic conditions favor the formation of SSAs (Nonaka & Sasaki, 2007). By combining these features, we can verify whether the subduction or spice injection is relevant to the anomalies on the isopycnals of 25-26 kg m^{-3}.

3.3.1 Midlatitude

Spiciness anomalies between 25-26 σ_θ are largely followed the pattern of temperature anomalies at around 60-120m, demonstrating the key role of temperature in regulating subsurface spiciness variability (Figures 10a and 10c). Salinity anomalies, however, enhance (weaken) the isopycnal spiciness variability when having the same (opposite) sign with temperature anomalies (Figures 10b and 10c). While interior temperature variability can almost be traced to the surface of outcrop, the salinity anomalies between 25-26 σ_θ are disconnected and appeared to lead surface variability, suggesting different dynamics are involved in the generation of anomalous signals associated with the two variables. Interior salinity variability in the region might relate to the propagation of subsurface salinity anomalies originate in the Gulf of Alaska (Pozo Buil & Di Lorenzo, 2015).

To characterize the contribution of subduction versus spice injection in the midlatitude, Figure 11 shows the maps of SSS, SST, and sea surface density in January-March (JFM) as well as the standard deviation of interannual spiciness anomalies between 25-26 σ_θ. The pivotal role of temperature on the isopycnal spiciness variability is confirmed as strong temperature gradients situate at the defined spiciness generation region, compared with the uniform change of SSS (Figures 11a and 11b). The σ_θ=25 isopycnal does expose to the surface and its annual wintertime outcrop position is largely located at the red box (Figure 11a). In addition, the mean outcrop line is well located at the area associated with the maximum standard deviation of interannual isopycnal spiciness variability (contour line of 0.12 kg m^{-3}, Figure 11c) while the extreme outcrop position extends further equatorward to the northern edge of the blue box. Therefore, subduction is expected to play a significant role in the formation of isopycnal spiciness anomalies in the midlatitude.

The contribution of the two processes is further clarified by the winter distribution of the isopycnal σ_θ=25 and the associated spiciness anomalies averaged between σ_θ=25-26 (Figure 12). The isopycnal σ_θ=25 displaces meridionally from its mean position of 39^0N which is largely associated with the variations of local SSTA. When the SSTA dominates and lack of meridional compensation between temperature and salinity (Figures 10a, 10b and 12), the surface temperature anomaly subducts and leaves its signature to the interior isopycnal spiciness anomalies. When the surface density is compensated by SST and SSS, the further the equatorward (poleward) migration is, the warmer (colder) and saltier (fresher) surface conditions are (Figures 11a and 11b), which subsequently induces positive (negative) interior signal (Figures 10c and 12). As a result, the winter peak of spiciness anomalies between 25-26 σ_θ is occasionally in or out of phase with the meridional displacement of the σ_θ=25 surface. However, subduction alone cannot fully explain the spiciness variability in the midlatitude North Pacific. The prolonged period of warm temperature anomalies at around 60-140m such as during 1993-1995, 1996-1997, 2005-2006 is associated with the persistence of temperature anomalies via the reemergence mechanism (Alexander & Deser, 1995), which reinforces the subsurface signal to the following winter and forms positive spiciness anomalies between 25-26 σ_θ (Figure 10). The perseverance of negative temperature anomalies during 1988-1991 hinders the downward penetration of positive surface signal in the following winter which in turn induces negative isopycnal spiciness anomalies. Therefore, subduction and reemergence are responsible for midlatitude isopycnal spiciness variability.

3.3.2 Subtropics

As σ_θ=25 surface has rarely outcropped (blue box, Figure 11), subduction is not the governing generation mechanism in this area. Contrary to the midlatitude, isopycnal spiciness variability here greatly follows the pattern of salinity anomalies (Figures 13b and 13c). For example, from 1985 to 1987, observed positive spiciness anomaly between σ_θ=25-26 kg m^{-3} is in tandem with positive salinity anomaly at around 120-240m while temperature shows an opposite signature during this period (Figures 13a and 13c). Because the isopycnal σ_θ=25 does not expose to the surface and the pivotal role of salinity to SSAs (Yeager & Large, 2004), injection is expected to play a role in the formation of spiciness anomalies in the region. During 1984-1985, a pulse of greater than normal salinity detrains the interior ocean, and subsequently forms subsurface warm/salty anomalies (Figures 13b and 13c). The penetration of fresher than normal pulse of salinity from the surface down to around 200m during 1997-1998 can also explain a large fraction of negative spiciness anomaly in the isopycnal surfaces 25-25.5 σ_θ. Therefore,

spice injection contributes considerably to isopycnal spiciness variability in the subtropical North Pacific.

However, a large fraction of salinity variation leading to isopycnal spiciness variability is not traceable to the surface, suggesting that other processes than spice injection are involved in the generation of SSAs. For example, the negative salinity anomaly during 1980-1982 is observed at a depth below 100m which is completely disconnected from the anomaly above (Figure 13b). This vertical discontinuity can also be found during 1982-1983, 1995-2002, and 2014-2017. These years are associated with strong and very strong El Niño events that can modulate the strength of the STC. In addition, decadal STC variability is strongly connected with PDO (Hong et al., 2014). The variability of AP in conjunction with strong spiciness gradient in the upstream area is favorable for the observed isopycnal spiciness formation (Figure 11d). This is consistent with studies that proposed the generation mechanism of anomalous advection across mean spiciness gradient (Kilpatrick et al., 2011) in the region characterized by strong lateral spiciness gradient (Yeager & Large, 2004) and prominent interannual to decadal variations of California Current (Chelton et al., 1982). Therefore, anomalous advection across mean spiciness gradient can be responsible for isopycnal spiciness variability in the eastern subtropics since a large fraction of salinity variation at depth is disconnected from the surface.

Generally, the boreal winter atmospheric forcing results in the formation of SSAs in the North Pacific. In the eastern midlatitude, the strengthening (weakening) of the AL drives a positive (negative) Qnet anomaly that induces the positive (negative) SSTAs (positive phase of the PDO). The sea surface density then migrates further poleward (equatorward). Depending upon the meridional compensation between SST and SSS, the resulting isopycnal spiciness anomaly can have the same or opposite sign as the SSTA. Both subduction and reemergence contribute to the formation of SSAs. In the subtropical Pacific, isopycnal spiciness variability is associated with the injection of surface information into the interior ocean due to net surface heat flux changes and the anomalous advection across mean spiciness gradient.

4 Discussion

The extratropical origin of spiciness anomalies in the central eastern equatorial Pacific is of great interest because of its key role in driving tropical climate variability (Gu & Philander, 1997; Schneider, 2000; Zeller et al., 2021). By artificially imposing continual interior perturbations in the western equatorial Pacific, Schneider (2004) showed that the arrival of spiciness signals can induce a modest coupled mode of ocean-atmosphere response in the tropics. The occurrences of subsurface warming during 2003-2005 and cooling during 2008-2010 in the central equatorial Pacific were hypothesized to initiate the weak 2004-2005 El Niño and strong 2010-2011 La Niña events (Li et al., 2012). In the present study, the extratropical spiciness anomalies likely impact tropical climate variability. The correlation between PC1 (real) and the Niño4 SST index when the former lead 13 months is -0.38 (Figure 14), consistent with the penetration of negative signal at lag +12 months (Figure 7). Although statistically significant at the 95% level according to a Student's t-test, the low correlation might relate to the long migration process. Therefore, to the extent of the present study, the leading spiciness mode is expected to impact tropical climate variability to a certain extent and potentially producing a decadal climate fluctuation in the North Pacific. Further investigation that employ coupled general circulation models with sufficiently long integration is needed to quantify the degree of extratropical subsurface influence on tropical climate.

The emergence of subsurface signals in the off-equatorial Pacific, resulting from the SSAs through the NPP, is also hypothesized to act as an oceanic "precursor" triggering the onset of ENSO (Ding et al., 2015). When these signals reach subtropical and tropical boundary, the STC and tropical dynamics start to play a role (Chen et al., 2015). There are consistent warm anomalies observed equatorward of 10^0N that precede those strong and very strong El Niño events over one year, except the moderate 2009-2010 ENSO (Figure 2). These positive anomalies in conjunction with the impact of the Victoria mode, defined as the second EOF of SSTAs poleward of 20^0N, may further initiate an anomalous signal of similar sign in the central eastern equatorial Pacific which eventually leads to the development of ENSO (Ding et al., 2015).

Apart from the downstream impact of extratropical signals, the interannual SST variability in the tropical Pacific can also feedback to the midlatitude subsurface variability through the atmospheric teleconnection. The highest correlations of PC1 (real) with Niño3 and Niño4 indices are 0.48 (PC1 lags 22 months) and 0.61 (PC1 lags 28 months), respectively (Figure 14). The regression maps of reconstructed spiciness anomalies using CEOF1 with the Niño3 (+22 months) and Niño4 (+28 months) SST indices account for a large fraction of the positive and negative subsurface signals in the midlatitude and subtropics, respectively (Figure S2), similar to the impacts of PDO (Figure 6a). The main difference between the PDO and tropical forcing is the negative anomaly centers at 40^0N, 150^0W that can only be explained by the former, confirming the primary role of extratropical air-sea interaction in driving spiciness mode. In addition, the contribution of Niño4 has a greater magnitude than Niño3, consistent with the twenty-first century shift toward a more Central Pacific (CP, here represented by Niño4) type of ENSO (Lee & McPhaden, 2010; McPhaden, 2012). These in turn generate decadal climate variability in the North Pacific that involves both oceanic and atmospheric bridges.

During 2013-2015, prolonged near-surface warming was observed in the northeastern Pacific, termed the "Pacific warm blob" (Bond et al., 2015) or marine heat wave (Frölicher et al., 2018; Oliver et al., 2018; Smale et al., 2019). The occurrence of this extraordinary phenomenon has been connected with different physical processes such as the coupling between the North Pacific Gyre Oscillation (NPGO) and PDO due to the two-way tropical-extratropical interactions via atmospheric teleconnection (Di Lorenzo & Mantua, 2016; Hu et al., 2017; Joh & Di Lorenzo, 2017), the tropical Northern Hemisphere (TNH) pattern in the atmosphere (Liang et al., 2017), and an extended weakening of the North Pacific High (Amaya et al., 2020). The "warm blob" overlies the region of interior spiciness formation in the midlatitude (Figure 7). During this period, prolonged positive temperature anomaly is observed at the surface down to over 250m (Hu et al., 2017) and precedes the positive surface salinity anomaly for around one year (Figures 10a and 10b). However, variations of salinity and temperature are almost in phase below 80m depth. As a result, the strongest warm/salty anomaly is produced in the interior ocean (Figure 10c). Given the strong connection between the warm blob and PDO (Joh & Di Lorenzo, 2017), and future projection of increasing variance of PDO under greenhouse forcing (Di Lorenzo & Mantua, 2016), the longer and more frequent occurrence of marine heat wave (Frölicher et al., 2018; Oliver et al., 2018) could lead to greater subsurface spiciness variability and stronger impact on Pacific climate variability (Tseng et al., 2017).

The SSAs between 25-26 σ_θ can amplify significantly during the downstream propagation, particularly from lag +12 to lag +48 months (Figure 7). Region of signal strengthening coincides with the North Pacific Eastern Subtropical Mode Water (NPESMW,

around 20-36^{0}N, 160-120^{0}W) formation (Hautala & Roemmich, 1998). The formation and dissipation of NPESMW can contribute to the isopycnal spiciness variability through the injection mechanism (Katsura, 2018), consistent with the present analysis (Figure 13). In addition, the NPESMW volume experiences significant decadal variability and is related to the PDO (Guo et al., 2018). Indeed, the PDO-associated atmospheric forcing produces Qnet anomalies in the subtropics, then impacts the NPESMW and ultimately subsurface spiciness variability. Therefore, NPESMW only serves as a bridge connecting the surface forcing to the interior variability. In other words, the PDO-related forcing effectively forces subsurface anomalies not only in the midlatitude but also extends further equatorward (Figures 4b and 6a).

5 Conclusions

This study shows strong connection between the PDO and subsurface spiciness variability in which during the positive (negative) phase of PDO, a dipole pattern of positive (negative) and negative (positive) SSAs is formed in the midlatitude and subtropics, respectively (Figure 15). The resulting anomalies then propagate equatorward along the NPP. The positive anomaly of midlatitude origin can reach 14^{0}N after 7 years of propagation while the negative anomaly of subtropical origin can arrive 10^{0}N after 3 years. In addition, a negative anomaly emerges after the occurrence of the midlatitude positive subsurface signal 2 year later, then follows the pathway that the positive takes to reach the western tropics. This ultimately leads to a decadal propagating mode of SSAs in the North Pacific. Further analysis demonstrates that the AL, the primary driver of the PDO, is responsible for the midlatitude subsurface spiciness variability by inducing a band of heat flux anomaly there.

In the eastern midlatitude North Pacific, isopycnal spiciness variability largely follows the pattern of temperature anomalies at around 60-120m depth. Spiciness anomalies between 25-26 σ_θ are generated via the subduction and reemergence. In contrast, isopycnal spiciness variability in the subtropics generally follows the variation of salinity anomalies at around 120-240m depth. Subduction plays no role in the interannual variability of spiciness signal as the isopycnal 25 σ_θ has never been exposed to the surface during the analysis period. Spice injection and anomalous advection across mean spiciness gradient are proposed as the two governing processes responsible for subsurface spiciness variability in the subtropical North Pacific.

Acknowledgments

This study was supported by the NSTC Grant 111-2111-M-002-015, Taiwan.

Open Research

The TEOS-10 used for the analysis is freely available at https://www.teos-10.org/software.htm. The CEOF routine can be obtained from http://hydr.ct.tudelft.nl/wbk/public/hooimeijer. Data sets used in this paper can be downloaded from the following.

EN422: https://www.metoffice.gov.uk/hadobs/en4/download-en4-2-2.html.

MOAA GPV: http://www.jamstec.go.jp/ARGO/J_ARGOe.html.

ERA5: https://www.ecmwf.int/en/forecasts/datasets/reanalysis-datasets/era5

References

Alexander, M. A. (1990). Simulation of the response of the North Pacific ocean to the anomalous atmospheric circulation associated with El Niño. *Clim Dynam*, *5*(1), 53-65. https://doi.org/10.1007/BF00195853.

Alexander, M. A. (1992). Midlatitude atmosphere-ocean interaction during El Niño. Part I: The North Pacific ocean. *J Climate*, *5*(9), 944-958. https://doi.org/10.1175/1520-0442(1992)005<0944:Maiden>2.0.Co;2.

Alexander, M. A., & Deser, C. (1995). A mechanism for the recurrence of wintertime midlatitude SST anomalies. *J Phys Oceanogr*, *25*(1), 122-137. https://doi.org/10.1175/1520-0485(1995)025<0122:Amftro>2.0.Co;2.

Amaya, D. J., Miller, A. J., Xie, S.-P., & Kosaka, Y. (2020). Physical drivers of the summer 2019 North Pacific marine heatwave. *Nature Communications*, *11*(1), 1903. https://doi.org/10.1038/s41467-020-15820-w.

Barnett, T. P. (1983). Interaction of the monsoon and Pacific trade wind system at interannual time scales Part I: The equatorial zone. *Monthly Weather Review*, *111*(4), 756-773. https://doi.org/10.1175/1520-0493(1983)111<0756:IOTMAP>2.0.CO;2.

Bond, N. A., Cronin, M. F., Freeland, H., & Mantua, N. (2015). Causes and impacts of the 2014 warm anomaly in the NE Pacific. *Geophys Res Lett*, *42*(9), 3414-3420. https://doi.org/10.1002/2015GL063306.

Capotondi, A., Alexander, M. A., Deser, C., & McPhaden, M. J. (2005). Anatomy and decadal evolution of the Pacific subtropical-tropical cells (STCs). *J Climate*, *18*(18), 3739-3758. https://doi.org/10.1175/jcli3496.1.

Chelton, D., Bernal, P., & McGowan, J. (1982). Large-scale interannual physical and biological interaction in the California Current (El Nino). *J Mar Res*, *40*.

Chen, H.-C., Sui, C.-H., Tseng, Y.-H., & Huang, B. (2015). An analysis of the linkage of Pacific subtropical cells with the recharge-discharge processes in ENSO evolution. *J Climate*, *28*(9), 3786-3805. https://doi.org/10.1175/jcli-d-14-00134.1.

Di Lorenzo, E., & Mantua, N. (2016). Multi-year persistence of the 2014/15 North Pacific marine heatwave. *Nature Climate Change*, *6*(11), 1042-1047. https://doi.org/10.1038/nclimate3082.

Ding, R., Li, J., Tseng, Y.-h., Sun, C., & Guo, Y. (2015). The Victoria mode in the North Pacific linking extratropical sea level pressure variations to ENSO. *Journal of Geophysical Research: Atmospheres*, *120*(1), 27-45. https://doi.org/10.1002/2014JD022221.

Fine, R. A., Peterson, W. H., & Ostlund, H. G. (1987). The penetration of tritium into the tropical Pacific. *J Phys Oceanogr*, *17*(5), 553-564. https://doi.org/10.1175/1520-0485(1987)017<0553:Tpotit>2.0.Co;2.

Flament, P. (2002). A state variable for characterizing water masses and their diffusive stability: spiciness. *Prog Oceanogr*, *54*(1), 493-501. https://doi.org/10.1016/S0079-6611(02)00065-4.

Frölicher, T. L., Fischer, E. M., & Gruber, N. (2018). Marine heatwaves under global warming. *Nature*, *560*(7718), 360-364. https://doi.org/10.1038/s41586-018-0383-9.

Fukumori, I., Lee, T., Cheng, B., & Menemenlis, D. (2004). The origin, pathway, and destination of Niño-3 water estimated by a simulated passive tracer and its adjoint. *J Phys Oceanogr*, *34*(3), 582-604. https://doi.org/10.1175/2515.1.

Furue, R., et al. (2015). Impacts of regional mixing on the temperature structure of the equatorial Pacific ocean. Part 1: Vertically uniform vertical diffusion. *Ocean Modelling*, *91*, 91-111. https://doi.org/10.1016/j.ocemod.2014.10.002.

Giese, B. S., Urizar, S. C., & Fučkar, N. S. (2002). Southern Hemisphere origins of the 1976 climate shift. *Geophys Res Lett*, *29*(2), 1-1-1-4. https://doi.org/10.1029/2001GL013268.

Good, S. A., Martin, M. J., & Rayner, N. A. (2013). EN4: Quality controlled ocean temperature and salinity profiles and monthly objective analyses with uncertainty estimates. *Journal of Geophysical Research: Oceans*, *118*(12), 6704-6716. https://doi.org/10.1002/2013JC009067.

Goodman, P. J., Hazeleger, W., de Vries, P., & Cane, M. (2005). Pathways into the Pacific equatorial undercurrent: A trajectory analysis. *J Phys Oceanogr*, *35*(11), 2134-2151. https://doi.org/10.1175/jpo2825.1.

Gu, D., & Philander, S. G. H. (1997). Interdecadal climate fluctuations that depend on exchanges between the tropics and extratropics. *Science*, *275*(5301), 805-807. https://doi.org/10.1126/science.275.5301.805.

Guo, Y., Lin, X., Wei, M., Liu, C., & Men, G. (2018). Decadal variability of North Pacific eastern subtropical mode water. *Journal of Geophysical Research: Oceans*, *123*(9), 6189-6206. https://doi.org/10.1029/2018JC013890.

Hasselmann, K. (1976). Stochastic climate models Part I. Theory. *Tellus*, *28*(6), 473-485. https://doi.org/10.1111/j.2153-3490.1976.tb00696.x.

Hautala, S. L., & Roemmich, D. H. (1998). Subtropical mode water in the northeast Pacific basin. *Journal of Geophysical Research: Oceans*, *103*(C6), 13055-13066. https://doi.org/10.1029/98JC01015.

Hazeleger, W., Visbeck, M., Cane, M., Karspeck, A., & Naik, N. (2001). Decadal upper ocean temperature variability in the tropical Pacific. *Journal of Geophysical Research: Oceans*, *106*(C5), 8971-8988. https://doi.org/10.1029/2000JC000536.

Hersbach, H., et al. (2020). The ERA5 global reanalysis. *Quarterly Journal of the Royal Meteorological Society*, *146*(730), 1999-2049. https://doi.org/10.1002/qj.3803.

Hong, L., Zhang, L., Chen, Z., & Wu, L. (2014). Linkage between the Pacific Decadal Oscillation and the low frequency variability of the Pacific subtropical cell. *Journal of Geophysical Research: Oceans*, *119*(6), 3464-3477. https://doi.org/10.1002/2013JC009650.

Horel, J. D. (1984). Complex principal component analysis: Theory and examples. *Journal of Applied Meteorology and Climatology*, *23*(12), 1660-1673. https://doi.org/10.1175/1520-0450(1984)023<1660:CPCATA>2.0.CO;2.

Hosoda, S., Ohira, T., & Nakamura, T. (2008). A monthly mean dataset of global oceanic temperature and salinity derived from Argo float observations. *JAMSTEC Report of Research and Development*, *8*, 47-59. https://doi.org/10.5918/jamstecr.8.47.

Hu, Z.-Z., Kumar, A., Jha, B., Zhu, J., & Huang, B. (2017). Persistence and predictions of the remarkable warm anomaly in the northeastern Pacific ocean during 2014-16. *J Climate*, *30*(2), 689-702. https://doi.org/10.1175/jcli-d-16-0348.1.

Huang, R. X. (2011). Defining the spicity. *J Mar Res*, *69*(4-6), 545-559. https://doi.org/10.1357/002224011799849390.

Huang, R. X., Yu, L. S., & Zhou, S. Q. (2018). New definition of potential spicity by the least square method. *J Geophys Res-Oceans*, *123*(10), 7351-7365. https://doi.org/10.1029/2018jc014306.

Huang, R. X., Yu, L. S., & Zhou, S. Q. (2021). Quantifying climate signals: Spicity, orthogonality, and distance. *J Geophys Res-Oceans*, *126*(2). https://doi.org/10.1029/2020JC016646.

Jackett, D. R., & Mcdougall, T. J. (1985). An oceanographic variable for the characterization of intrusions and water masses. *Deep-Sea Res*, *32*(10), 1195-1207. https://doi.org/10.1016/0198-0149(85)90003-2.

Joh, Y., & Di Lorenzo, E. (2017). Increasing coupling between NPGO and PDO leads to prolonged marine heatwaves in the northeast Pacific. *Geophys Res Lett*, *44*(22), 11,663-611,671. https://doi.org/10.1002/2017GL075930.

Johnson, G. C., & McPhaden, M. J. (1999). Interior pycnocline flow from the subtropical to the equatorial Pacific ocean. *J Phys Oceanogr*, *29*(12), 3073-3089. https://doi.org/10.1175/1520-0485(1999)029<3073:Ipffts>2.0.Co;2.

Katsura, S. (2018). Properties, formation, and dissipation of the North Pacific eastern subtropical mode water and its impact on interannual spiciness anomalies. *Prog Oceanogr*, *162*, 120-131. https://doi.org/10.1016/j.pocean.2018.02.023.

Kilpatrick, T., Schneider, N., & Di Lorenzo, E. (2011). Generation of low-frequency spiciness variability in the thermocline. *J Phys Oceanogr*, *41*(2), 365-377. https://doi.org/10.1175/2010jpo4443.1.

Kolodziejczyk, N., & Gaillard, F. (2012). Observation of spiciness interannual variability in the Pacific pycnocline. *J Geophys Res-Oceans*, *117*. https://doi.org/10.1029/2012JC008365.

Kuntz, L. B., & Schrag, D. P. (2018). Hemispheric asymmetry in the ventilated thermocline of the tropical Pacific. *J Climate*, *31*(3), 1281-1288. https://doi.org/10.1175/jcli-d-17-0686.1.

Lee, T., Fukumori, I., Menemenlis, D., Xing, Z., & Fu, L.-L. (2002). Effects of the Indonesian throughflow on the Pacific and Indian oceans. *J Phys Oceanogr*, *32*(5), 1404-1429. https://doi.org/10.1175/1520-0485(2002)032<1404:Eotito>2.0.Co;2.

Lee, T., & McPhaden, M. J. (2010). Increasing intensity of El Niño in the central-equatorial Pacific. *Geophys Res Lett*, *37*(14). https://doi.org/10.1029/2010GL044007.

Li, Y. L., Wang, F., & Sun, Y. (2012). Low-frequency spiciness variations in the tropical Pacific ocean observed during 2003-2012. *Geophys Res Lett*, *39*. https://doi.org/10.1029/2012GL053971.

Liang, Y.-C., Yu, J.-Y., Saltzman, E. S., & Wang, F. (2017). Linking the tropical northern hemisphere pattern to the Pacific warm blob and Atlantic cold blob. *J Climate*, *30*(22), 9041-9057. https://doi.org/10.1175/jcli-d-17-0149.1.

Liu, Z. (1994). A simple model of the mass exchange between the subtropical and tropical ocean. *J Phys Oceanogr*, *24*(6), 1153-1165. https://doi.org/10.1175/1520-0485(1994)024<1153:Asmotm>2.0.Co;2.

Liu, Z., & Huang, B. (1998). Why is there a tritium maximum in the central equatorial Pacific thermocline? *J Phys Oceanogr*, *28*(7), 1527-1533. https://doi.org/10.1175/1520-0485(1998)028<1527:Witatm>2.0.Co;2.

678 Liu, Z., Philander, S. G. H., & Pacanowski, R. C. (1994). A GCM study of tropical-subtropical upper-ocean water
679 exchange. *J Phys Oceanogr*, *24*(12), 2606-2623. https://doi.org/10.1175/1520-
680 0485(1994)024<2606:Agsotu>2.0.Co;2.
681 Liu, Z., & Shin, S.-I. (1999). On thermocline ventilation of active and passive tracers. *Geophys Res Lett*, *26*(3), 357-
682 360. https://doi.org/10.1029/1998GL900315.
683 Lu, P., & McCreary, J. P. (1995). Influence of the ITCZ on the flow of thermocline water from the subtropical to the
684 equatorial Pacific ocean. *J Phys Oceanogr*, *25*(12), 3076-3088. https://doi.org/10.1175/1520-
685 0485(1995)025<3076:Iotiot>2.0.Co;2.
686 Lu, P., McCreary, J. P., & Klinger, B. A. (1998). Meridional circulation cells and the source waters of the Pacific
687 equatorial undercurrent. *J Phys Oceanogr*, *28*(1), 62-84. https://doi.org/10.1175/1520-
688 0485(1998)028<0062:Mccats>2.0.Co;2.
689 Luo, Y. Y., Rothstein, L. M., Zhang, R. H., & Busalacchi, A. J. (2005). On the connection between South Pacific
690 subtropical spiciness anomalies and decadal equatorial variability in an ocean general circulation model. *J*
691 *Geophys Res-Oceans*, *110*(C10). https://doi.org/10.1029/2004JC002655.
692 Lyon, B., Barnston, A. G., & DeWitt, D. G. (2014). Tropical Pacific forcing of a 1998-1999 climate shift:
693 observational analysis and climate model results for the boreal spring season. *Clim Dynam*, *43*(3), 893-909.
694 https://doi.org/10.1007/s00382-013-1891-9.
695 Mantua, N. J., Hare, S. R., Zhang, Y., Wallace, J. M., & Francis, R. C. (1997). A Pacific interdecadal climate
696 oscillation with impacts on salmon production. *Bulletin of the American Meteorological Society*, *78*(6),
697 1069-1080. https://doi.org/10.1175/1520-0477(1997)078<1069:Apicow>2.0.Co;2.
698 McCreary, J. P., & Lu, P. (1994). Interaction between the subtropical and equatorial ocean circulations: The
699 subtropical cell. *J Phys Oceanogr*, *24*(2), 466-497. https://doi.org/10.1175/1520-
700 0485(1994)024<0466:Ibtsae>2.0.Co;2.
701 McDougall, T. J., Barker, P. M., & Stanley, G. J. (2021). Spice variables and their use in physical oceanography.
702 *Journal of Geophysical Research: Oceans*, *126*(2), e2019JC015936.
703 https://doi.org/10.1029/2019JC015936.
704 McDougall, T. J., & Klocker, A. (2010). An approximate geostrophic streamfunction for use in density surfaces.
705 *Ocean Modelling*, *32*(3), 105-117. https://doi.org/10.1016/j.ocemod.2009.10.006.
706 McDougall, T. J., & Krzysik, O. A. (2015). Spiciness. *J Mar Res*, *73*(5), 141-152.
707 https://doi.org/10.1357/002224015816665589.
708 McPhaden, M. J. (2012). A 21st century shift in the relationship between ENSO SST and warm water volume
709 anomalies. *Geophys Res Lett*, *39*(9). https://doi.org/10.1029/2012GL051826.
710 McPhaden, M. J., & Fine, R. A. (1988). A dynamical interpretation of the tritium maximum in the central equatorial
711 Pacific. *J Phys Oceanogr*, *18*(10), 1454-1457. https://doi.org/10.1175/1520-
712 0485(1988)018<1454:Adiott>2.0.Co;2.
713 Munk, W. (1981), Internal waves and small-scale processes, edited.
714 Nie, X., Gao, S., Wang, F., & Qu, T. (2016). Subduction of North Pacific tropical water and its equatorward
715 pathways as shown by a simulated passive tracer. *Journal of Geophysical Research: Oceans*, *121*(12),
716 8770-8786. https://doi.org/10.1002/2016JC012305.
717 Nonaka, M., & Sasaki, H. (2007). Formation mechanism for isopycnal temperature-salinity anomalies propagating
718 from the eastern South Pacific to the equatorial region. *J Climate*, *20*(7), 1305-1315.
719 https://doi.org/10.1175/Jcli4065.1.
720 O'Kane, T. J., Matear, R. J., Chamberlain, M. A., & Oke, P. R. (2014). ENSO regimes and the late 1970's climate
721 shift: The role of synoptic weather and South Pacific ocean spiciness. *J Comput Phys*, *271*, 19-38.
722 https://doi.org/10.1016/j.jcp.2013.10.058.
723 Oliver, E. C. J., et al. (2018). Longer and more frequent marine heatwaves over the past century. *Nature*
724 *Communications*, *9*(1), 1324. https://doi.org/10.1038/s41467-018-03732-9.
725 Pierce, D. W., Barnett, T. P., & Latif, M. (2000). Connections between the Pacific ocean tropics and midlatitudes on
726 decadal timescales. *J Climate*, *13*(6), 1173-1194. https://doi.org/10.1175/1520-
727 0442(2000)013<1173:Cbtpot>2.0.Co;2.
728 Pozo Buil, M., & Di Lorenzo, E. (2015). Decadal changes in Gulf of Alaska upwelling source waters. *Geophys Res*
729 *Lett*, *42*(5), 1488-1495. https://doi.org/10.1002/2015GL063191.
730 Rodgers, K. B., Cane, M. A., Naik, N. H., & Schrag, D. P. (1999). The role of the Indonesian throughflow in
731 equatorial Pacific thermocline ventilation. *Journal of Geophysical Research: Oceans*, *104*(C9), 20551-
732 20570. https://doi.org/10.1029/1998JC900094.

Rothstein, L. M., Zhang, R.-H., Busalacchi, A. J., & Chen, D. (1998). A numerical simulation of the mean water pathways in the subtropical and tropical Pacific ocean. *J Phys Oceanogr*, *28*(2), 322-343. https://doi.org/10.1175/1520-0485(1998)028<0322:Ansotm>2.0.Co;2.

Sasaki, Y. N., Schneider, N., Maximenko, N., & Lebedev, K. (2010). Observational evidence for propagation of decadal spiciness anomalies in the North Pacific. *Geophys Res Lett*, *37*. https://doi.org/10.1029/2010GL042716.

Schneider, N. (2000). A decadal spiciness mode in the tropics. *Geophys Res Lett*, *27*(2), 257-260. https://doi.org/10.1029/1999gl002348.

Schneider, N. (2004). The response of tropical climate to the equatorial emergence of spiciness anomalies. *J Climate*, *17*(5), 1083-1095. https://doi.org/10.1175/1520-0442(2004)017<1083:Trotct>2.0.Co;2.

Schneider, N., & Cornuelle, B. D. (2005). The forcing of the Pacific Decadal Oscillation. *J Climate*, *18*(21), 4355-4373. https://doi.org/10.1175/jcli3527.1.

Schneider, N., Miller, A. J., Alexander, M. A., & Deser, C. (1999a). Subduction of decadal North Pacific temperature anomalies: Observations and dynamics. *J Phys Oceanogr*, *29*(5), 1056-1070. https://doi.org/10.1175/1520-0485(1999)029<1056:Sodnpt>2.0.Co;2.

Schneider, N., Venzke, S., Miller, A. J., Pierce, D. W., Barnett, T. P., Deser, C., & Latif, M. (1999b). Pacific thermocline bridge revisited. *Geophys Res Lett*, *26*(9), 1329-1332. https://doi.org/10.1029/1999GL900222.

Schott, F. A., Mccreary Jr., J. P., & Johnson, G. C. (2004), Shallow overturning circulations of the tropical-subtropical oceans, in *Earth's Climate*, edited, pp. 261-304, doi:https://doi.org/10.1029/147GM15.

Smale, D. A., et al. (2019). Marine heatwaves threaten global biodiversity and the provision of ecosystem services. *Nature Climate Change*, *9*(4), 306-312. https://doi.org/10.1038/s41558-019-0412-1.

Stephens, M., Liu, Z., & Yang, H. (2001). Evolution of subduction planetary waves with application to North Pacific decadal thermocline variability. *J Phys Oceanogr*, *31*(7), 1733-1746. https://doi.org/10.1175/1520-0485(2001)031<1733:Eospww>2.0.Co;2.

Stommel, H. (1962). On the cause of the temperature-salinity curve in the ocean. *Proceedings of the National Academy of Sciences*, *48*(5), 764-766. https://doi.org/10.1073/pnas.48.5.764.

Tailleux, R., Lazar, A., & Reason, C. J. C. (2005). Physics and dynamics of density-compensated temperature and salinity anomalies. Part I: Theory. *J Phys Oceanogr*, *35*(5), 849-864. https://doi.org/10.1175/Jpo2706.1.

Tatebe, H., Imada, Y., Mori, M., Kimoto, M., & Hasumi, H. (2013). Control of decadal and bidecadal climate variability in the tropical Pacific by the off-equatorial South Pacific ocean. *J Climate*, *26*(17), 6524-6534. https://doi.org/10.1175/jcli-d-12-00137.1.

Tseng, Y.-H., Ding, R., & Huang, X.-m. (2017). The warm blob in the northeast Pacific-the bridge leading to the 2015/16 El Niño. *Environmental Research Letters*, *12*(5), 054019. https://doi.org/10.1088/1748-9326/aa67c3.

Veronis, G. (1972). On properties of seawater defined by temperature, salinity, and pressure. *J Mar Res*.

Wang, Y. Y., & Luo, Y. Y. (2020). Variability of spice injection in the upper ocean of the southeastern Pacific during 1992-2016. *Clim Dynam*, *54*(5-6), 3185-3200. https://doi.org/10.1007/s00382-020-05164-y.

Yang, H., Jiang, H., & Tan, B. (2005). Asymmetric impact of the North and South Pacific on the equator in a coupled climate model. *Geophys Res Lett*, *32*(5). https://doi.org/10.1029/2004GL022195.

Yeager, S. G., & Large, W. G. (2004). Late-winter generation of spiciness on subducted isopycnals. *J Phys Oceanogr*, *34*(7), 1528-1547. https://doi.org/10.1175/1520-0485(2004)034<1528:LGOSOS>2.0.CO;2.

Yu, J.-Y., & Kim, S. T. (2011). Relationships between extratropical sea level pressure variations and the central Pacific and eastern Pacific types of ENSO. *J Climate*, *24*(3), 708-720. https://doi.org/10.1175/2010jcli3688.1.

Zeller, M., McGregor, S., van Sebille, E., Capotondi, A., & Spence, P. (2021). Subtropical-tropical pathways of spiciness anomalies and their impact on equatorial Pacific temperature. *Clim Dynam*, *56*(3), 1131-1144. https://doi.org/10.1007/s00382-020-05524-8.

Zhang, R.-H., & Liu, Z. (1999). Decadal thermocline variability in the North Pacific ocean: Two pathways around the subtropical gyre. *J Climate*, *12*(11), 3273-3296. https://doi.org/10.1175/1520-0442(1999)012<3273:Dtvitn>2.0.Co;2.

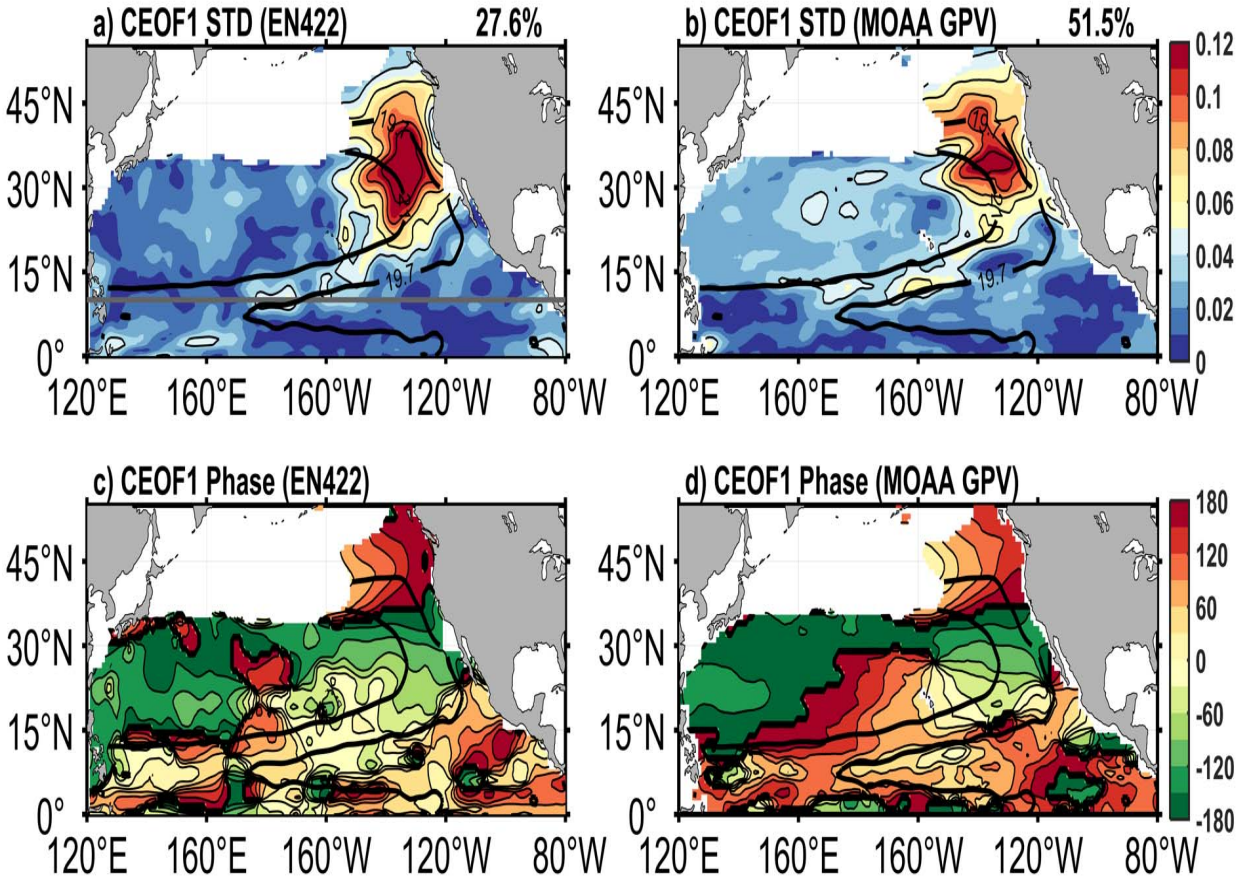

Figure 1. Standard deviation of low-frequency spiciness variability (kg m^{-3}) between 25-26 σ_θ in the North Pacific associated with CEOF1. The variance explained by CEOF1 is shown in (a) for EN422 and (b) for MOAA GPV, respectively. The spatial phase (in degree) of the leading mode derived from (c) EN422 and (d) MOAA GPV. The thick black lines denote the mean AP of 19.7- and 21.0 m^2s^{-2} (NPP). The gray line in (a) indicates the latitude of 10^0N.

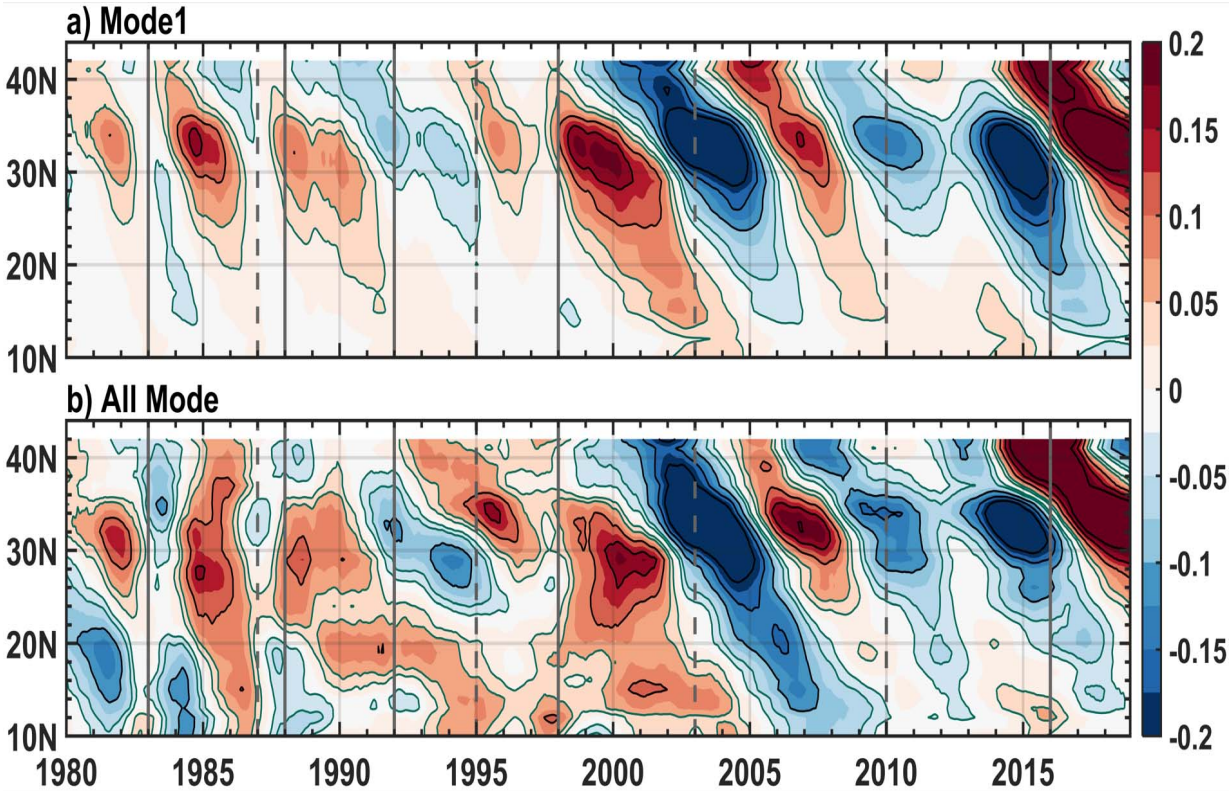

Figure 2. Latitude-time diagram of reconstructed spiciness anomalies (kg m^{-3}) using the (a) first and (b) all CEOF modes averaged along the NPP. The vertical solid (dashed) gray lines represent strong and very strong (moderate) El Nino events that peak in January based on the Oceanic Niño Index (ONI).

784

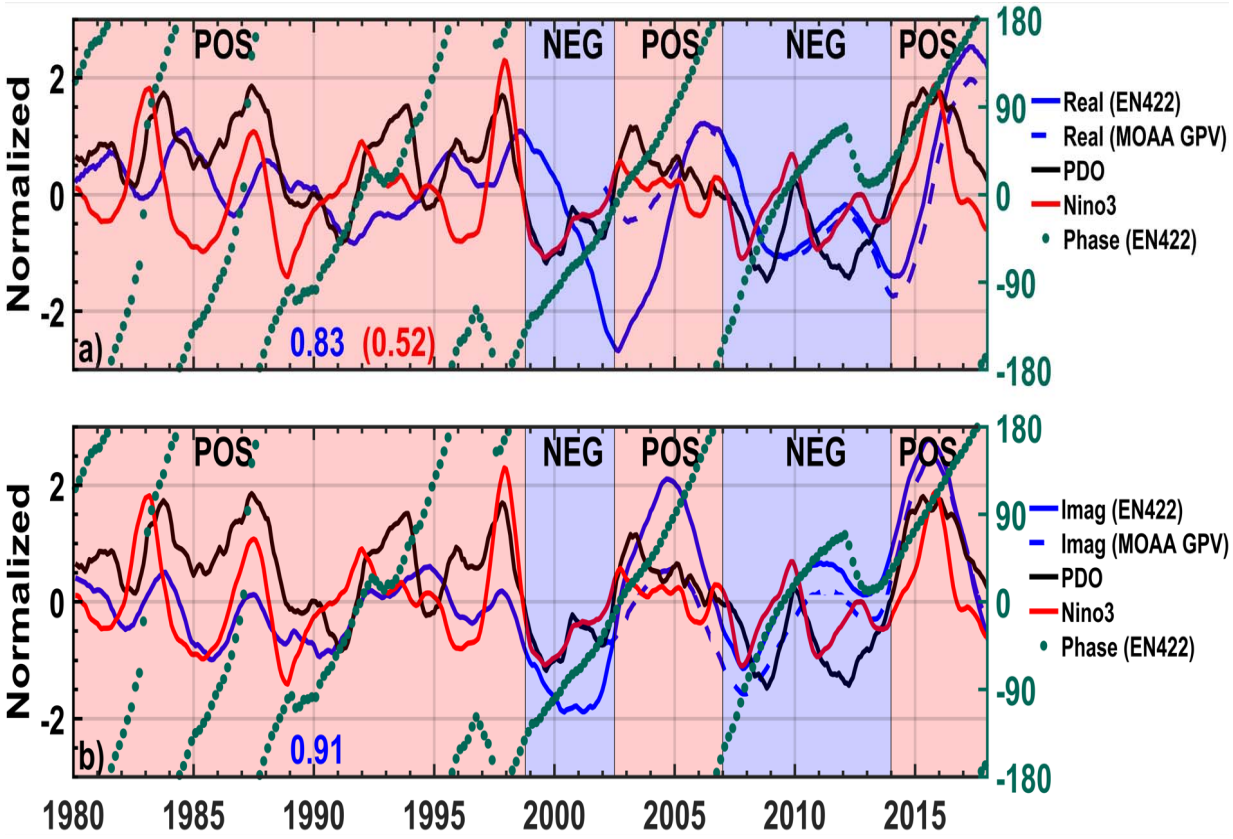

Figure 3. Normalized time series of (a) real and (b) imaginary expansion coefficients of CEOF1. The associated temporal phase (in degree) of the CEOF1 is shown as green dots. The black and red lines are the PDO index from the NOAA Physical Sciences Laboratory (PSL, https://psl.noaa.gov/pdo/) and Niño3 (5^0S–5^0N, 150^0–90^0W) index obtained from the NOAA Climate Prediction Center (http://www.cpc.noaa.gov/products/analysis_monitoring/ensostuff/ensoyears.shtml), respectively. The blue number in (a) is the simultaneous correlation between PC1 (real) of spiciness anomalies derived from MOAA GPV and EN422 during the same period (2002-2018) and similarly, the number in (b) is the correlation between the first imaginary part of the two datasets. The second number in (a) is the simultaneous correlation between PDO and the Niño3 index (red). POS and NEG correspond to PDO positive and negative phases.

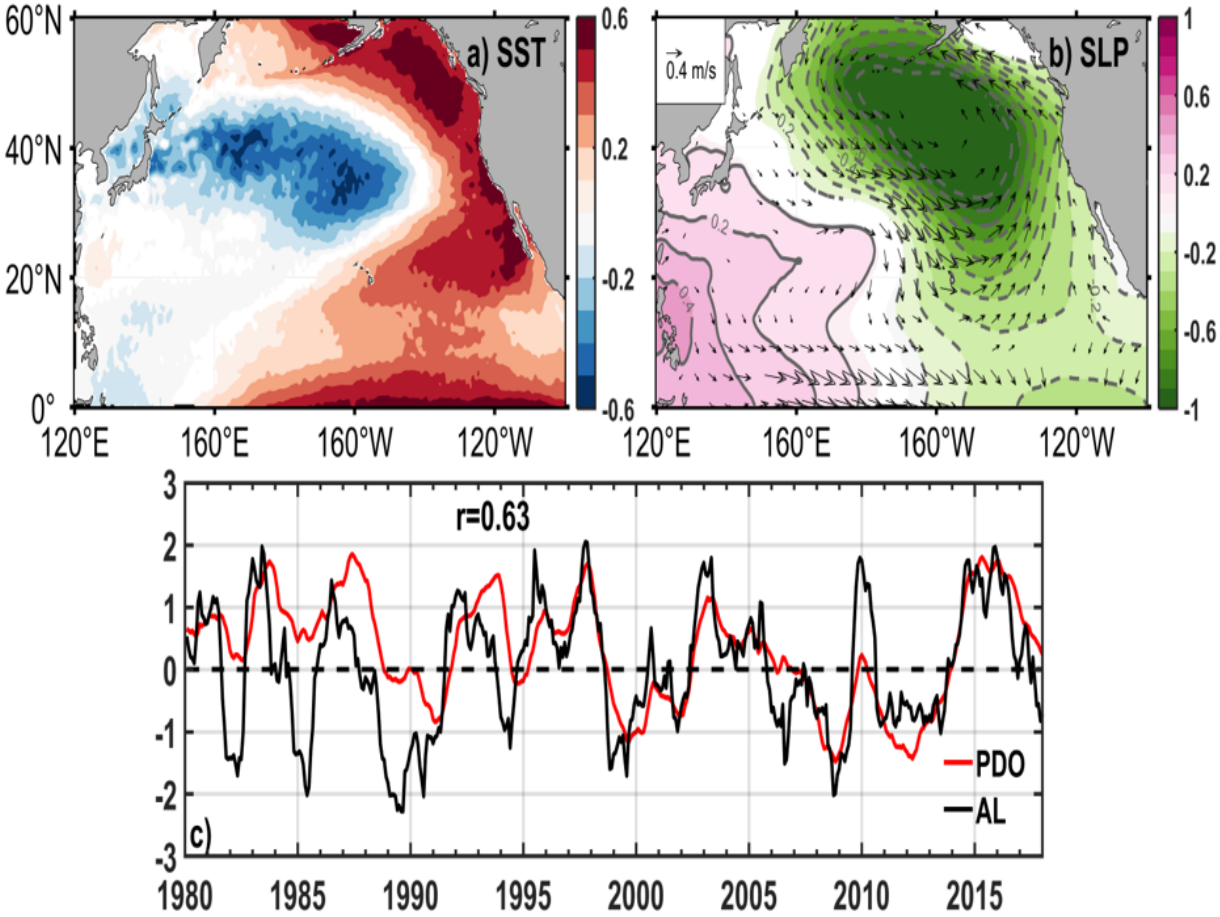

coefficients that are statistically significant at 95% level (Student's t-test). In all panels, positive lags indicate PDO leads the spiciness anomalies.

785

Figure 5. Pacific (a) SSTAs (^{0}C) and (b) SLPAs (hPa, shading and gray contours) regressed with the PDO index. Wind vectors at 10 m regressed with the PDO index are also imposed in (b). Only regressed values significant at the 95% level (Student's t-test) are shown. (c) Time series of the AL (black, PC1 of the EOF analysis of interannual SLPAs between 20^0-60^{0}N, 120^{0}E-80^{0}W. The first EOF mode explains 41% of the total SLP variance and the second EOF mode accounts for 19%). The red curve is the PDO index. The simultaneous correlation between AL and PDO is 0.63.

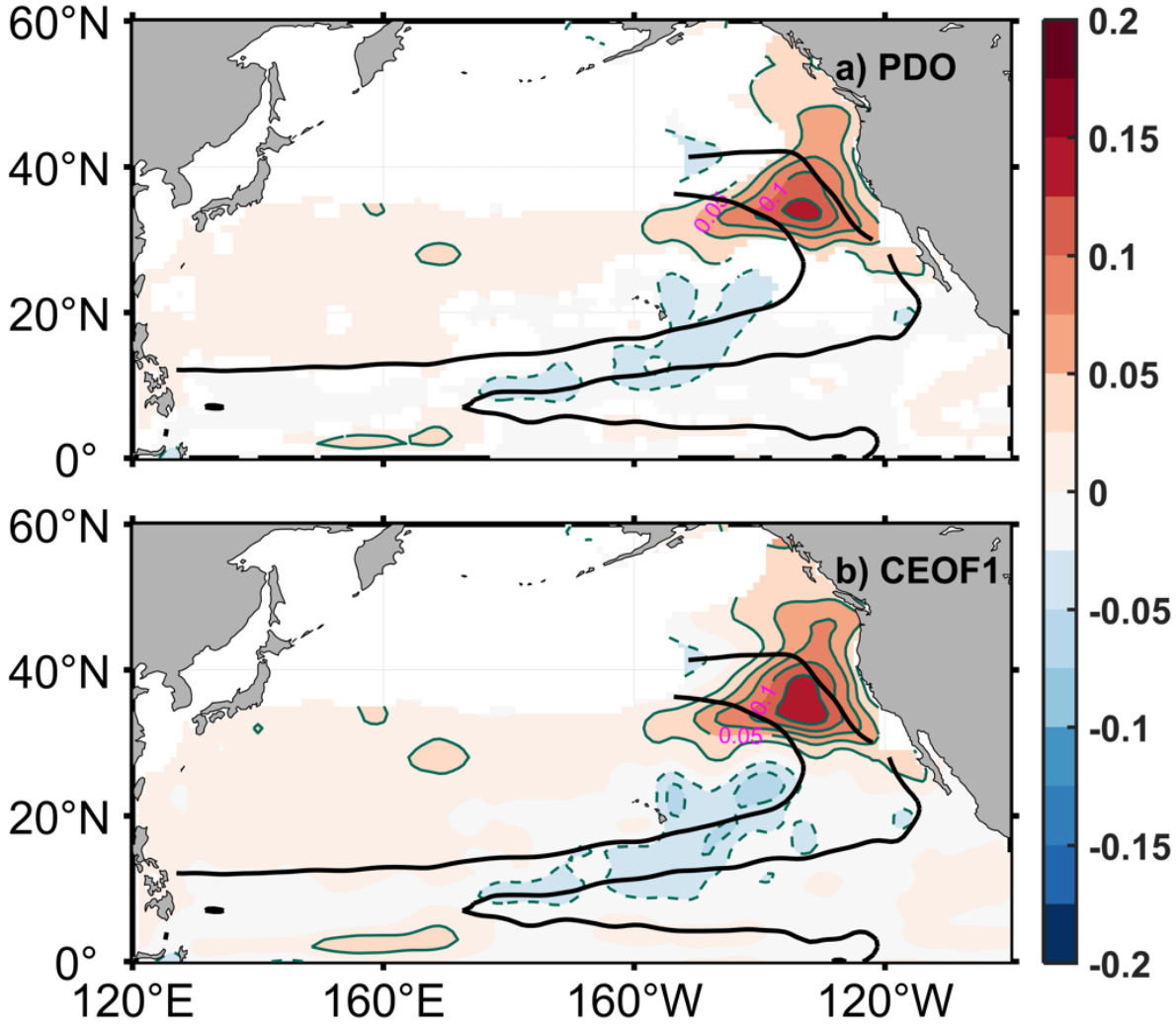

Figure 6. (a) Reconstructed spiciness anomalies using CEOF1 regressed with the PDO index at lag +22 months (shading and green contours, only regressed values significant at the 95% level according to a Student's t-test are shown). The contour interval is 0.025 kg m^{-3} and solid contours denote positive anomaly while dashed contours denote negative anomaly. (b) Spatial structure of CEOF1 (real). The thick black lines represent the NPP.

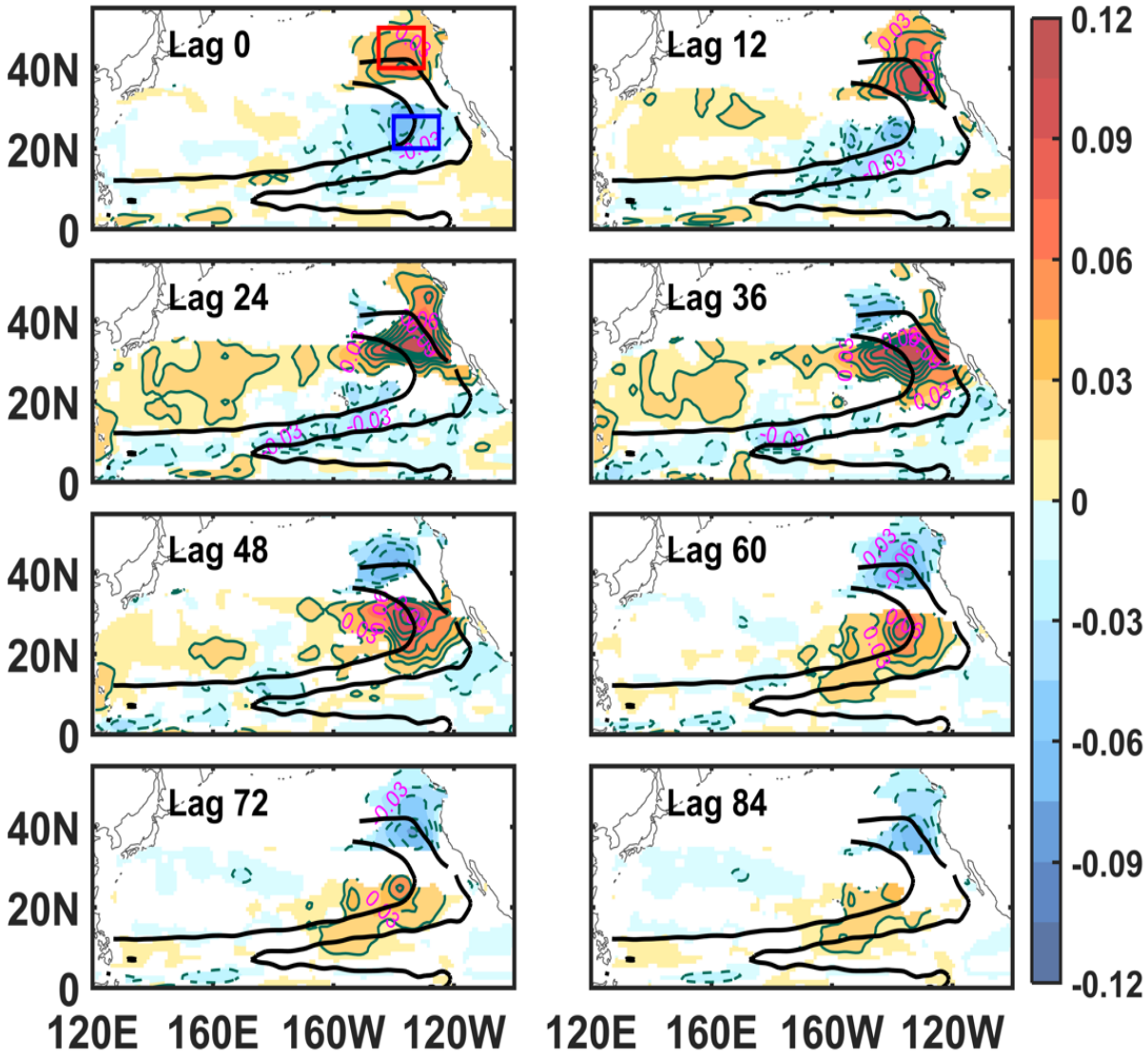

Figure 7. Reconstructed spiciness anomalies using CEOF1 regressed with the PDO index from lag 0 to lag +84 months (shading and green contours, only regression significant at the 95% level according to a Student's t-test are shown). The contour interval is 0.015 kg m^{-3} and solid contours denote positive anomaly while dashed contours denote negative anomaly. Positive lags indicate PDO leads the spiciness anomalies. The red and blue boxes represent the midlatitude (40-50^{0}N, 145-130^{0}W) and subtropical (20-28^{0}N, 140-125^{0}W) regions, respectively. The thick black lines represent the NPP.

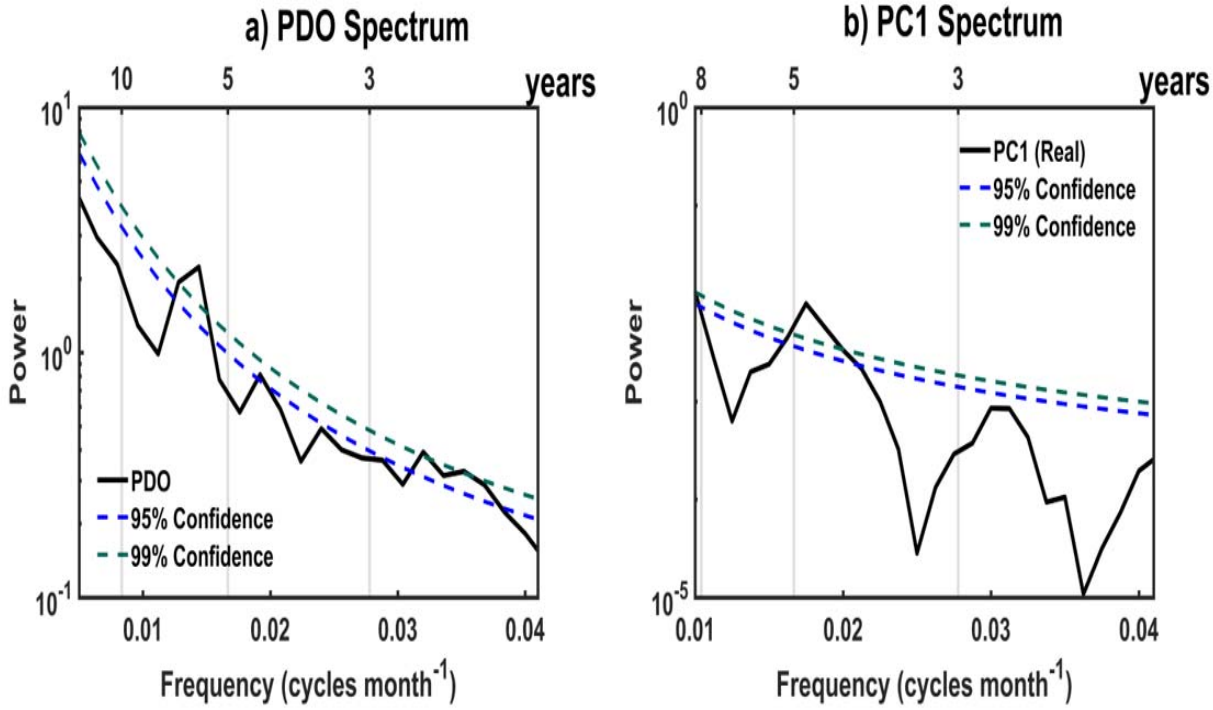

Figure 8. Power spectra of the (a) PDO index and (b) PC1 (real) of spiciness anomalies. The PDO index used for spectral analysis is from 1948-2019. Dashed blue and green curves denote the corresponding 95% and 99% red noise confidence levels.

788

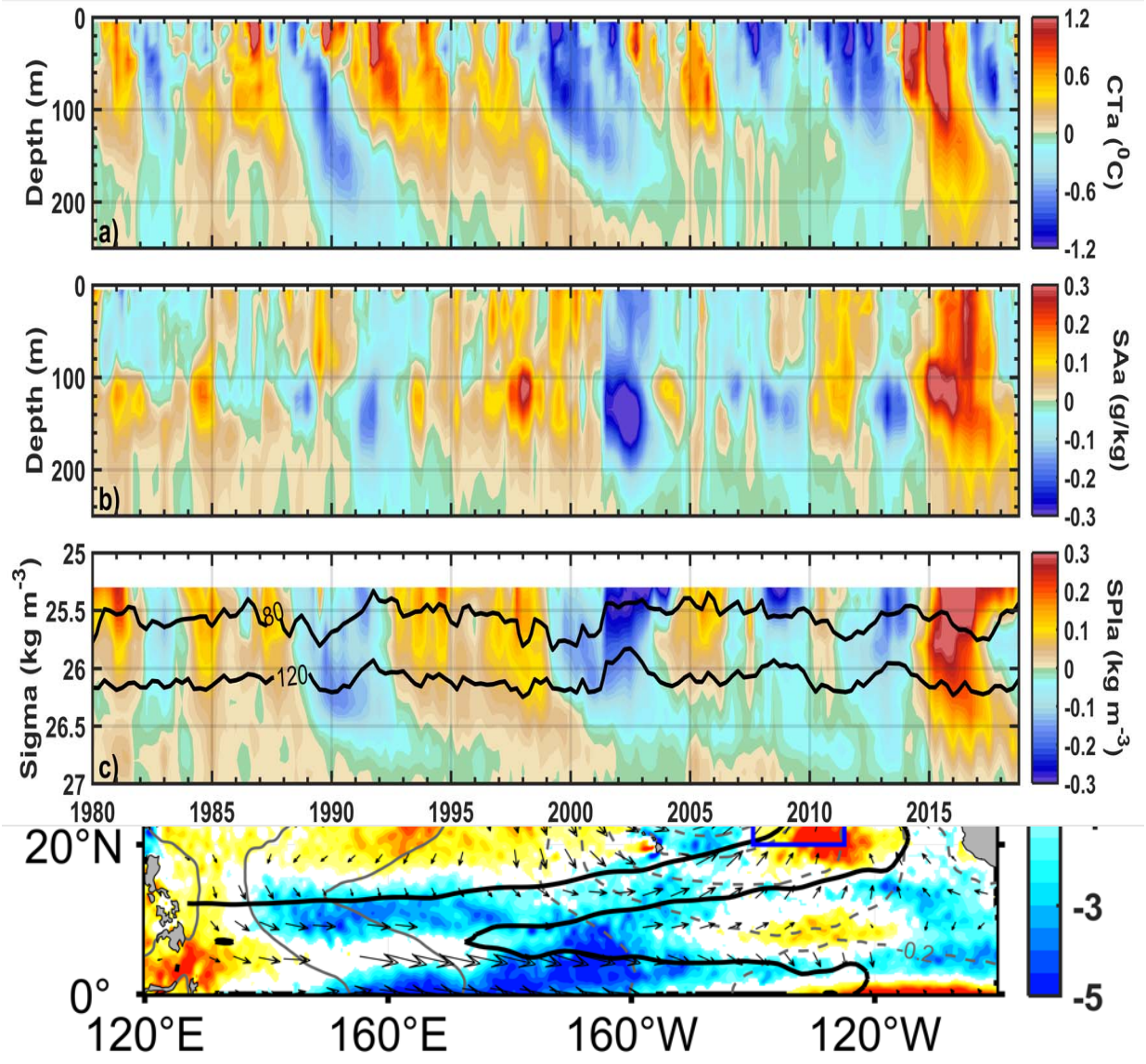

Figure 9. (a) SLP (hPa, shading and gray contours) and (b) Qnet (W m^{-2}, shading) anomalies regressed with the PC1 of spiciness anomalies. Wind vectors at 10 m regressed with the PC1 are also imposed. Regressed values significant at the 95% level (Student's t-test) are shaded for SLP and Qnet anomalies. Only regressed wind vectors significant at the 95% level are shown. The red and blue boxes are described in Figure 7. The thick black lines represent the NPP.

789

Figure 10. Time-depth plot of (a) CT and (b) SA anomalies averaged in 40-50^{0}N, 145-130^{0}W (red box in Figure 7) over three consecutive months (January-March, April-June, July-September, and October-December). (c) Time-sigma plot of spiciness anomalies (SPIa) averaged over the same region and period as (a) and (b).

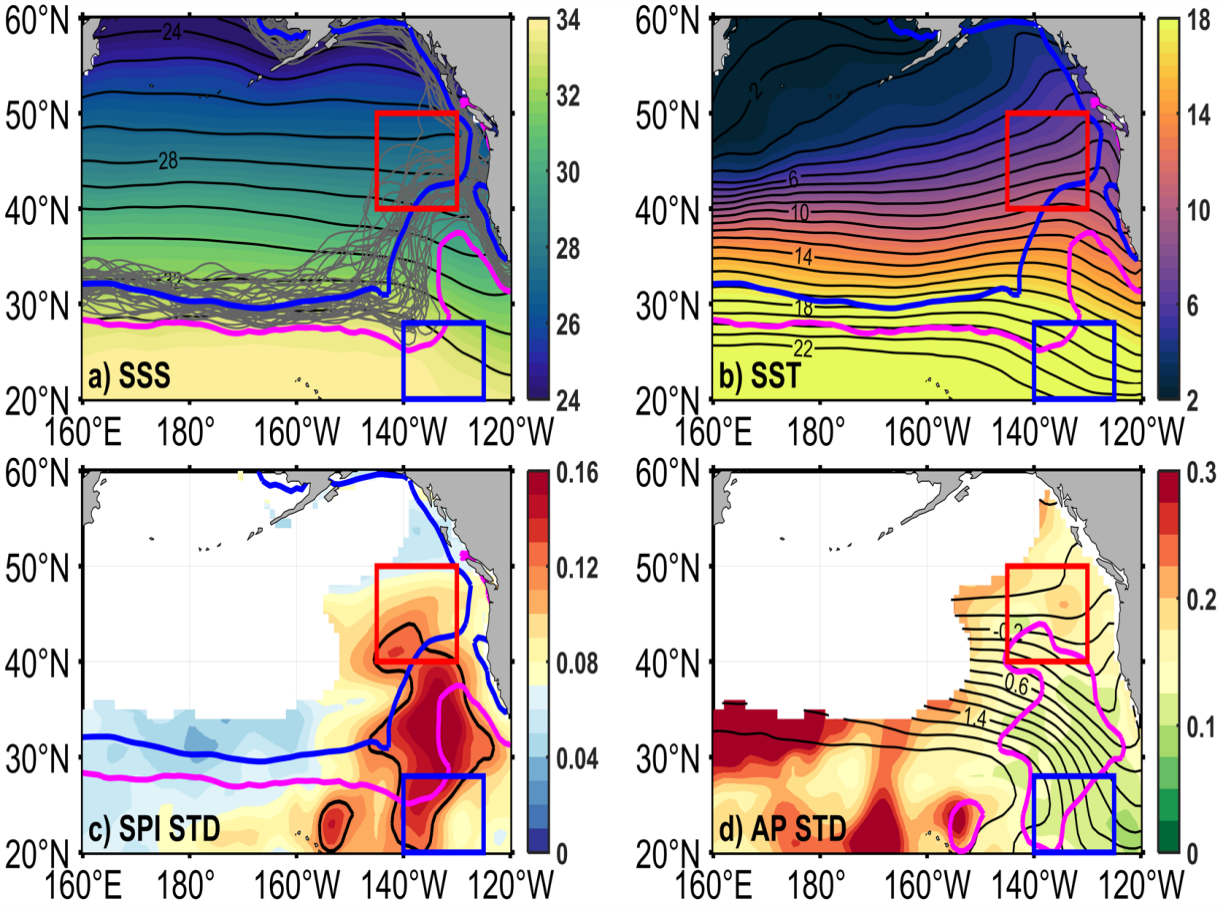

790

Figure 11. Mean JFM (a) SSS (g/kg, shading and black contours) and (b) SST (^{0}C, shading and black contours). Standard deviation of the interannual (c) spiciness (kg m^{-3}) and (d) AP (m^{2}s^{-2}) anomalies averaged between 25-26 σ_θ. Thin gray contours in (a) denote the mean JFM outcrop position of σ_θ=25 surface for an individual year during the analysis period while thick blue and magenta in (a), (b) and (c) denote the mean (1980-2018) and extreme equatorward outcrop position of σ_θ=25, respectively. The black and magenta contours in (c) and (d) indicate standard deviation of SPIa greater than 0.12 kg m^{-3}, respectively. Contours in (d) are the mean spiciness averaged between 25-26 σ_θ. The red and blue boxes are the regions defined in Figure 7.

791

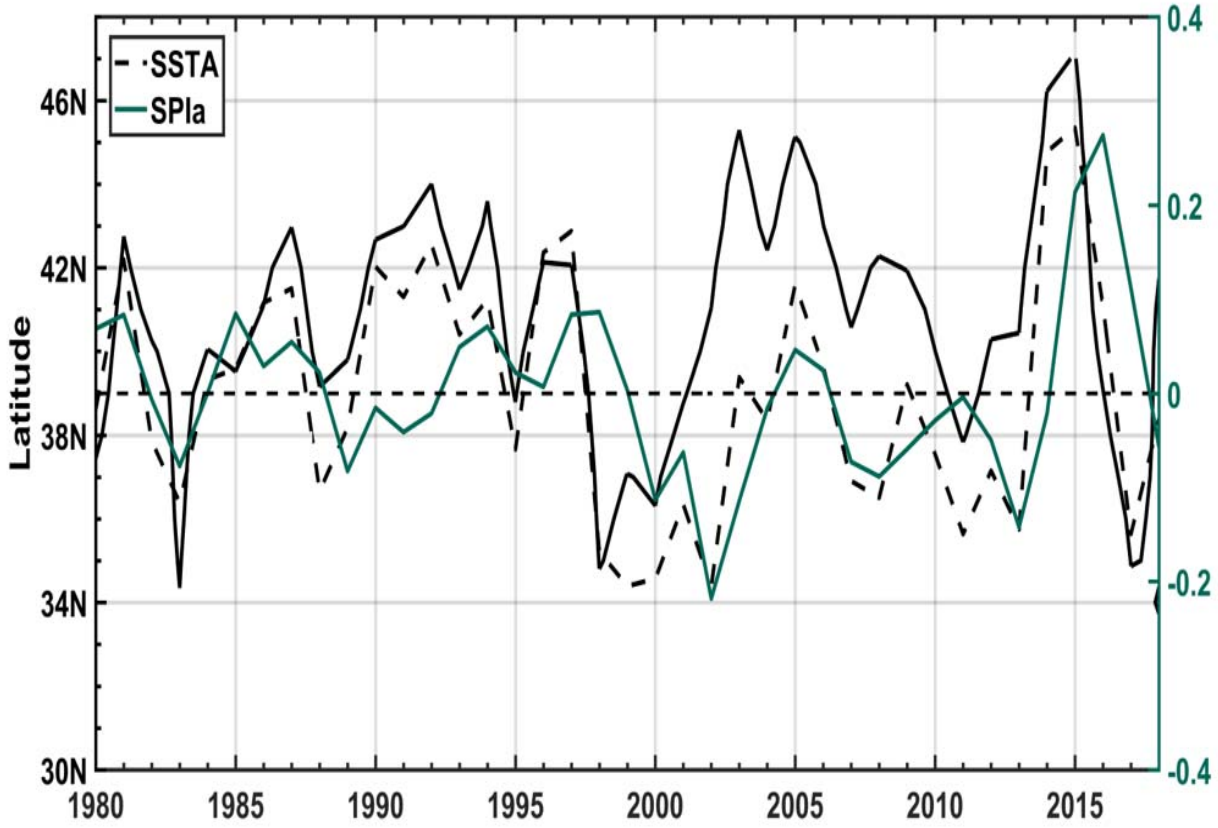

Figure 12. Time series of outcrop latitude of σ_θ=25 averaged from 145^0 to 130^{0}W (left, black solid line). The black dashed line is the mean area (32-48^{0}N, 145-130^{0}W) SSTA (right, ^{0}C). The green solid line is the mean area (red box) SPIa (right, kg m^{-3}) averaged between 25-26 σ_θ. SSTA is reduced by a factor of 0.25 for easy comparison. All the time series are based on mean JFM fields.

792

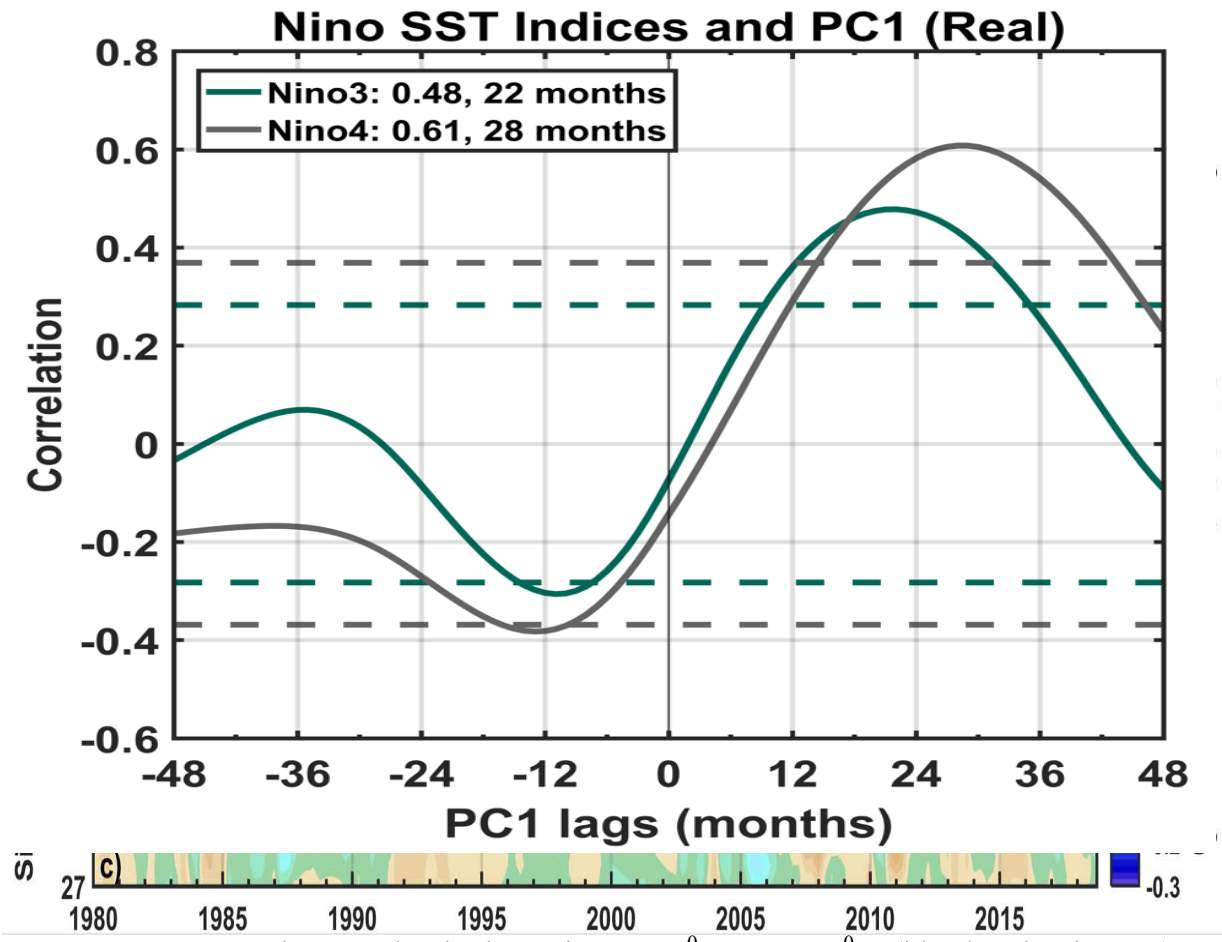

Figure 13. Same as Figure 10 but in the region 20-28^{0}N, 140-125^{0}W (blue box in Figure 7).

793

Figure 14. Lead-lag correlation coefficients between Nino SST indices and the PC1 of spiciness anomalies. The Niño3 and Niño4 (5^0S–5^0N, 160^0E–150^0W) indices are obtained from the NOAA Climate Prediction Center. Positive lags indicate the Nino SST indices lead the PC1.

794

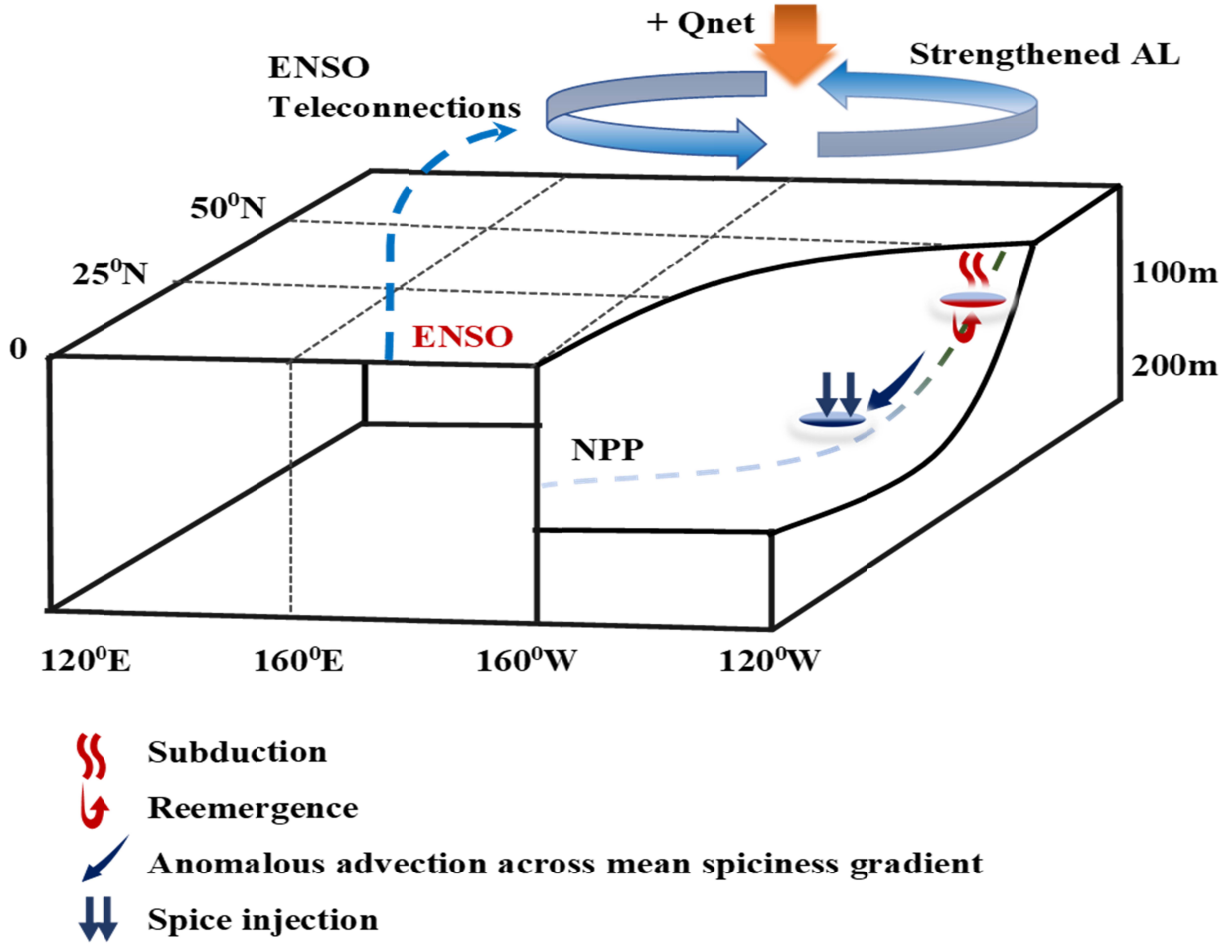

Figure 15. Framework of decadal spiciness mode in the North Pacific. Red (dark blue) circle indicates positive (negative) spiciness anomalies in the midlatitude (subtropics).

795